Seafloor character of the Roman Rock area in False Bay, South Africa.

Non-peer-reviewed preprint submitted to EarthArXiv

Andrew Terhorst[a] and John Rogers[b]

[a]Commonwealth Scientific and Industrial Research Organisation, Hobart, Australia;

[b]Department of Geology, University of Cape Town, Rondebosch, South Africa

ARTICLE HISTORY

Compiled February 25, 2025

ABSTRACT

Context: This study investigates the seafloor character of a 12 km^2 area off Simon's Town in False Bay, South Africa.

Aims: The goal was to map the seafloor geology around Roman Rock Lighthouse, focusing on sedimentology.

Methods: Side-scan sonar and single-beam echosounder were used, complemented by sediment sampling and diver observations for ground-truthing. Sediment samples were analysed for texture and composition.

Key Results: Six patterns of reflectivity (acoustic facies) were identified, including granite outcrops, wave ripples, and patches of gravelly and quartzose sands. Sediment analysis showed a mix of calcareous and quartzose components, with calcareous material dominating the gravel fraction near granite outcrops.

Conclusions: The Roman Rock seafloor reflects a complex depositional environment shaped by biogenic activity and wave-induced sediment transport.

Implications: This research lays the groundwork for future geological studies in False Bay, particularly around wave-induced sediment dynamics.

KEYWORDS

False Bay; South Africa; seafloor mapping; side-scan sonar; diver observations

CONTACT Andrew Terhorst. Email: andrew.terhorst@csiro.au

1. Introduction

This paper revisits and updates an earlier, unpublished study (Terhorst, 1988) that explored the seafloor geology around the Roman Rock lighthouse, located in the northwest corner of False Bay, South Africa. The initial investigation employed side-scan sonar and single-beam echosounder technologies to map the area's seafloor geology, complemented by grab samples and diver inspections to validate the sonar interpretations. This revision summarises the foundational work and re-examines its conclusions using recent geological and physical oceanographic data, providing a contemporary perspective on the findings. Recognising that technological advancements can reshape our methodologies, this paper argues for the enduring value of earlier techniques when applied thoughtfully and supplemented with new information. We aim to bridge the gap between past and present research, renewing interest in the seafloor geology of False Bay and underlining the importance of continuous exploration in marine science.

Numerous geological studies have been conducted in False Bay, offering a comprehensive understanding of the region. Research covering the entire bay includes works by Morgans (1956),Bowie (1966),Simpson, Du Plessis and Forder (1970),Gentle (1971),Flemming (1982), and Du Plessis and Glass (1991). Other studies have focused on specific areas within False Bay: Retief's 1970 research focuses on sediment transport patterns in Gordon's Bay (Retief, 1970). At the same time, Flemming (1976) explores the evolution of Rocky Bank at the entrance of False Bay. Erosion of the northern shoreline, particularly around Strandfontein and Monwabisi Beach, has been studied by Schoonees, Scholtz, Van Tonder, Moller and Lenhoff (1983), Fourie, Ansorge, Backeberg, Cawthra, MacHutchon and van Zyl (2015), and MacHutchon (2015). Van Zyl (2011) documented a side-scan sonar survey along the western shore that forms part of the Table Mountain Marine Protected Area. This localised study, originally commissioned by the Institute for Maritime Technology (IMT) on behalf of the South African Navy Hydrographic Office, stands out as one of the more detailed geological explorations in False Bay.

As to the organisation of this paper, the following section describes the physical setting of False Bay. This description covers (a) the physiography of the bay, (b) its seafloor geology, and (c) various aspects of the bay's physical oceanography. The paper then

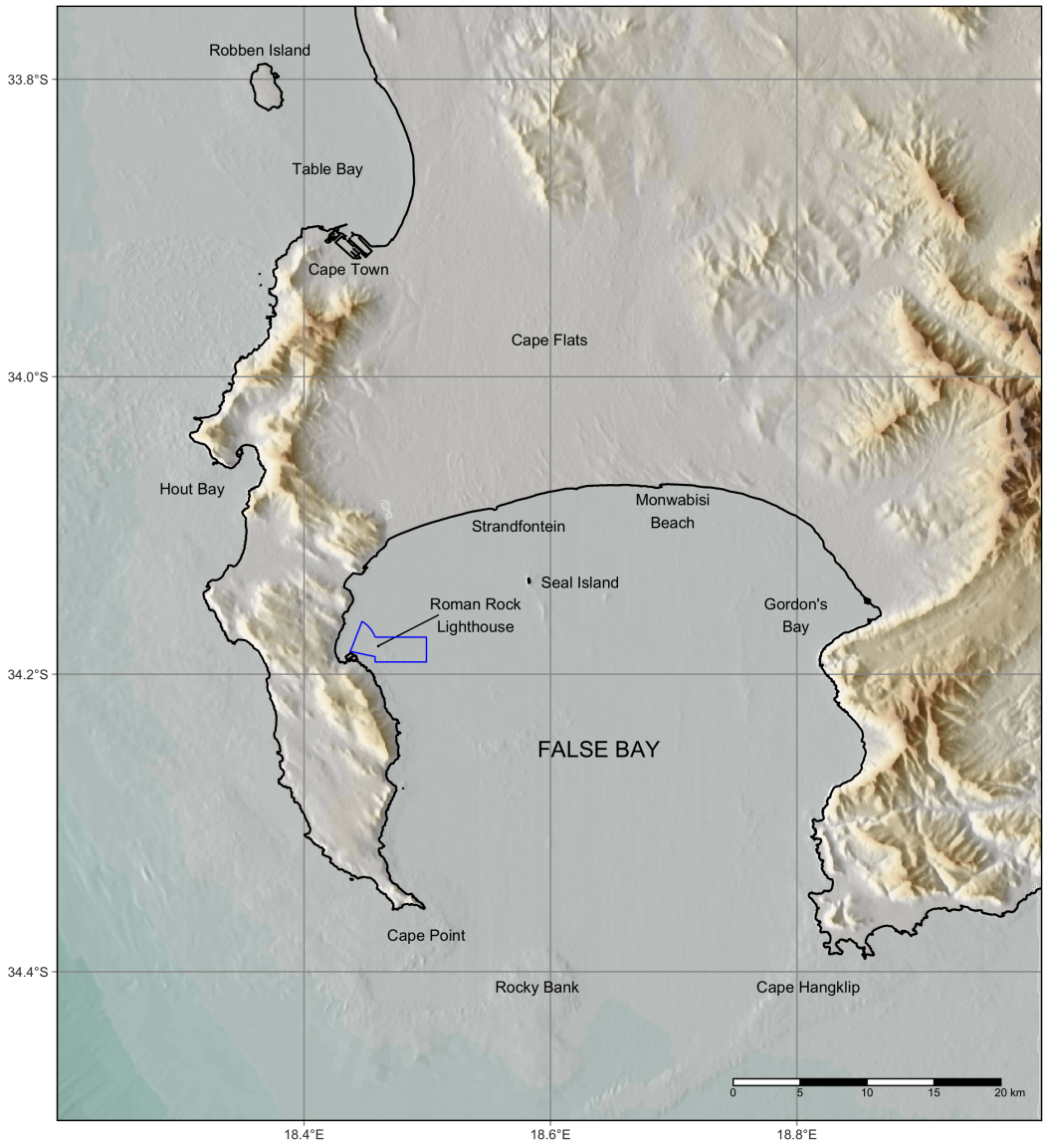

Figure 1. Shaded relief map showing the location of the study area (outlined in blue) off Simon's Town in the NW corner of False Bay. Note the steep mountains to the west and north of the survey area that significantly influence the wind regime across False Bay. Rocky Bank focuses the energy of long-period swells entering the bay.

explains how the data in the Roman Rock area were collected and processed, followed by a presentation and discussion of the results of the data analysis. It concludes with a summary of the main findings and recommendations for further research.

2. Physical setting

False Bay is the southward extension of a broad sandy valley known as the "Cape Flats" situated between the mountainous Cape Peninsula to the west and the Hottentots-Holland Mountains to the east (Figure 1). The seafloor within the bay slopes at a gradient of 1:370 toward the south, reaching a depth of over 100m between Cape Point and Cape Hangklip (Du Plessis and Glass, 1991; Glass and Du Plessis, 1976; Rogers, 2018). Apart from rock pinnacles and reefs around Roman Rock, Seal Island, York Shoal, East Shoal, and Whittle Rock, the seafloor in the western and southern parts of the Bay is relatively smooth, unlike the seafloor in the eastern part, which is more irregular (Du Plessis and Glass, 1991). Rocky Bank is a shallow reef at the entrance to False Bay that affects how ocean swells enter the Bay.

2.1. Geology

The geology of False Bay is inferred from onshore geological maps, hand-contoured hydrographic survey fair-charts, dredge and grab samples, and from magnetometer, shallow seismic and side-scan sonar traverses (Du Plessis and Glass, 1991).

2.1.1. Bedrock geology

Cambrian ($\sim$ 540 my) Cape Peninsula Granite underlies the western half of False Bay. The Cape Peninsula Granite intruded the Cambrian ($\sim$ 560 my) Malmesbury Supergroup shale that underlies the eastern half of False Bay (Belcher and Kisters, 2003; Scheepers and Schoch, 2006). The Ordovician Table Mountain Group's erosion-resistant sandstone overlies the Cape Peninsula Granite and Malmesbury Supergroup. The sandstone forms the mountainous terrain flanking the western and eastern sides of False Bay (Theron, 1984).

The granite outcrops along the coast south of Simon's Town tend to be blocky and

well-jointed with deep weathering in places (Rogers, 2018, p. 253 – 274). Seismic profiles show that False Bay's granite is deeply weathered in places. Joint spacing probably controls the depth of weathering – the closer the spacing, the deeper the weathering (Linton, 1955). Granite outcrops are more likely to occur where joints are more widely spaced (Glass, 1977).

Roman Rock lighthouse, situated in the middle of the study area, is built on top of a large granite tor that protrudes above the sea surface (Figure 2). South of Simon's Town, the unconformity between the Cape Peninsula Granite and the Table Mountain Group is about 100 metres above the current sea level (viz. Rogers (2018, p.64)). The unconformity dips below sea level north of Simon's Town, suggesting the bedrock in the northwestern corner of the study area is likely part of the Table Mountain Group.

The Cape Peninsula Granite and lower parts of the Table Mountain Group have been intruded by a swarm of dolerite dykes (Haughton, 1933). The dyke swarm dates to the Early Cretaceous and is thought to be associated with the opening of the South Atlantic (Backeberg, Reid, Trumbull and Romer, 2011). Magnetometer data indicate the presence of a large WNW-ESE trending dolerite dyke in the Cape Peninsula Granite beneath the study area (Simpson et al., 1970).

2.1.2. Unconsolidated sediments

Much of the seafloor in the western half of False Bay is covered by sediment, unlike the seafloor in the eastern half of the bay, which is mostly exposed Tygerberg Formation siltstone (Du Plessis and Glass, 1991). Seismic profiles indicate that the unconsolidated sediment is more than 10 m thick in the middle of False Bay. However, it is less than 2m thick in the study area (Du Plessis and Glass, 1991). Flemming (1982) analysed 190 sediment samples collected in False Bay by Bowie (1966) and Glass and Gasson (1980). Four of these samples were collected within the study area. The unconsolidated sediment is mostly fine to medium sand, except around granite outcrops, which are composed of coarse bioclastic material. According to Flemming (1982), bottom-traction is the primary sediment movement mechanism in the study area's western part. In the deeper eastern part of the study area, the primary mechanism for sediment movement is lower-bottom suspension.

Figure 2. Roman Rock lighthouse – December 2022. The cast-iron lighthouse was built in 1861 on top of a granite tor that protrudes above the sea surface at low tide. Note the north-facing solar panels that power the lighthouse. Simon's Town appears in the background at the base of the 678m high Swartberg mountain. Image credit: Andrew Morson.

2.2. Physical oceanography

2.2.1. Wind regime

Weather patterns at the SW tip of Africa are influenced by the interaction between the South Atlantic Anticyclone (SAA), situated in the subtropical high-pressure belt, and westerly (Rossby) waves in the circumpolar low-pressure belt (Schulze, 1965). The position of the SAA oscillates between a southern hemisphere summer mean of 32°S and a winter mean of 28°S. False Bay, at about 34°S, is dominated by anticyclonic conditions in summer and by cyclonic conditions in winter (Jury, 2020). Consequently, the physical oceanography of False Bay is dominated by a bidirectional wind regime, with winds blowing seasonally from opposing quarters. Figure 3 depicts the monthly wind speed distribution and wind direction in False Bay. It is based on ERA5 monthly averaged data on single levels from 1979 to the present (Hersbach, Bell, Berrisford, Hirahara, Horányi, Muñoz-Sabater, Nicolas, Peubey, Radu, Schepers et al., 2020). The Bay is dominated by SE winds from October to April and by NW winds from May to September. SE winds tend to blow harder than the NW winds.

The mountainous terrain of the Cape Peninsula strongly influences wind patterns in False Bay (Jury, 2020). As Figure 1 shows, mountains shield the study area from strong NW winds. However, the same mountains also channel strong SE winds (Coleman, Diedericks, Theron and Lencart e Silva, 2021). Gale-force SE winds can generate rough seas across the study area.

2.3. Thermal structure

Atkins (1970*a*) was the first to analyse the thermal structure of False Bay. His data show that sea-surface temperatures (SSTs) in the study area range from 20.3 °C in summer to 14.8 °C in winter. Bottom temperatures in the study area range between 12.2 °C in summer to 14.3 °C in winter. Recent circulation models support earlier conclusions that the pronounced thermocline observed in summer is caused by SE winds pushing warmer surface water into the Bay (Coleman et al., 2021; Grundlingh and Potgieter, 1993; Wainman, Polito and Nelson, 1987).

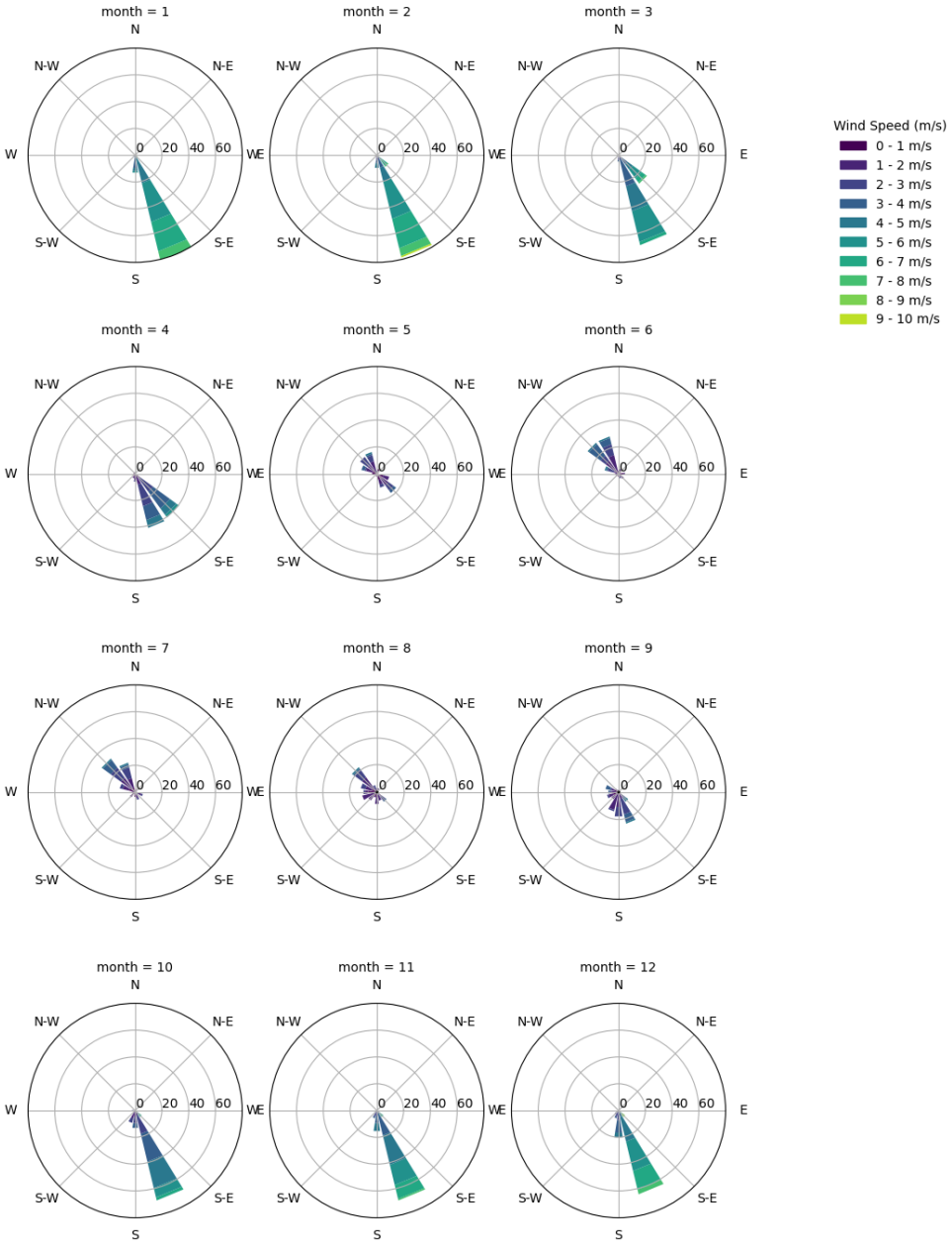

Figure 3. ERA5 monthly average wind speed and direction in False Bay. ERA5 is the fifth generation European Centre for Medium-Range Weather Forecasts (ECMWF) reanalysis for global climate and weather.

2.4. Tidal regime

Analysis of historical tide-gauge data shows that Simon's Town experiences a spring-tide range of 1.486 meters. False Bay falls into a semi-diurnal upper micro-tidal (<2 m tidal-range) environment (Davies, 1980; Grundlingh and Largier, 1991; Stephenson, 2016). With such a regime, tidal currents are expected to be relatively weak in the study area (Rautenbach, Barnes and de Vos, 2019; Vos, Vichi and Rautenbach, 2021). Data from an Acoustic Doppler Current Profiler (ADCP) deployed off Miller's Point, six kilometres south of Simon's Town, show that tide-driven bottom currents never exceed 0.1 ms^{-1} (Coleman et al., 2021).

2.5. Swell regime

Southwesterly swells dominate the southwest coast of South Africa (Figure 4). The Cape Peninsula provides a natural barrier protecting much of False Bay from the direct impact of these swells. Rocky Bank, at the mouth of False Bay, focuses the energy of southwesterly swells on the rocky eastern shoreline of False Bay, as detailed in studies by Shipley (1964), Darbyshire (1966), and more recently by Salonen and Rautenbach (2021).

Southerly swells, originating from deep low-pressure systems south of the country, occasionally penetrate the bay. These swells, too, are concentrated by Rocky Bank, but their impact is felt predominantly along the northwest shore of False Bay (Bang, 1967; Darbyshire, 1966). This concentration of energy can cause considerable damage to coastal structures, as documented by MacHutchon (2015) and Pfaff, Logston, Raemaekers, Hermes, Blamey, Cawthra, Colenbrander, Crawford, Day, Du Plessis et al. (2019). The eastern half of our study area lies directly in the path of these focused southerly swells (Figure 5).

Data from the above-mentioned ADCP show that wave heights in the northwest corner of False Bay can reach 1.5 m (Daniels, Fearon, Vilaplana, Hewitson and Rautenbach, 2022). However, such wave heights tend to be associated with shorter-period waves between 4 s and 6 s, typically generated by strong local winds.

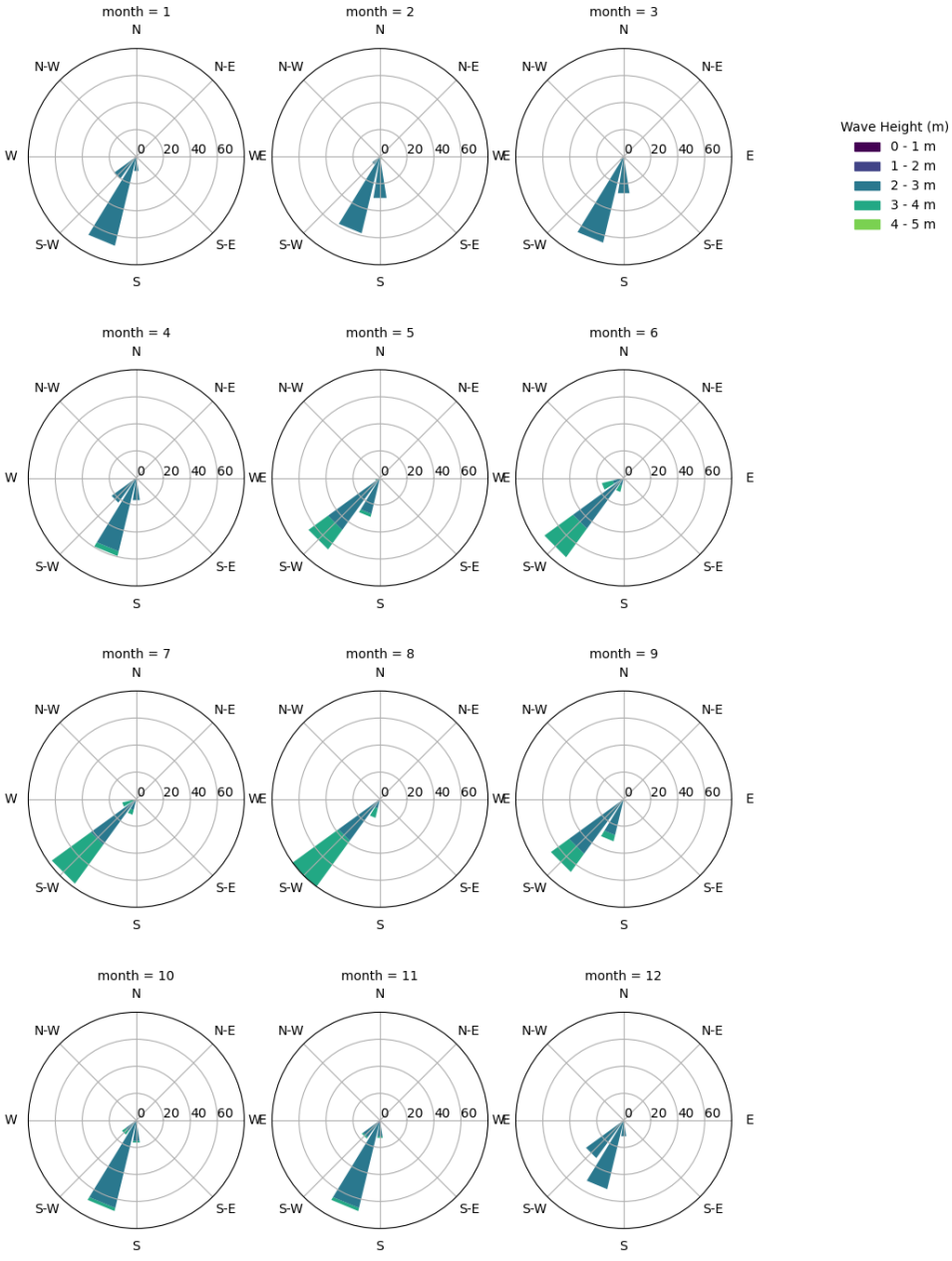

Figure 4. ERA5 monthly average swell height and direction at the SW tip of Africa. Southwesterly swells dominate the region.

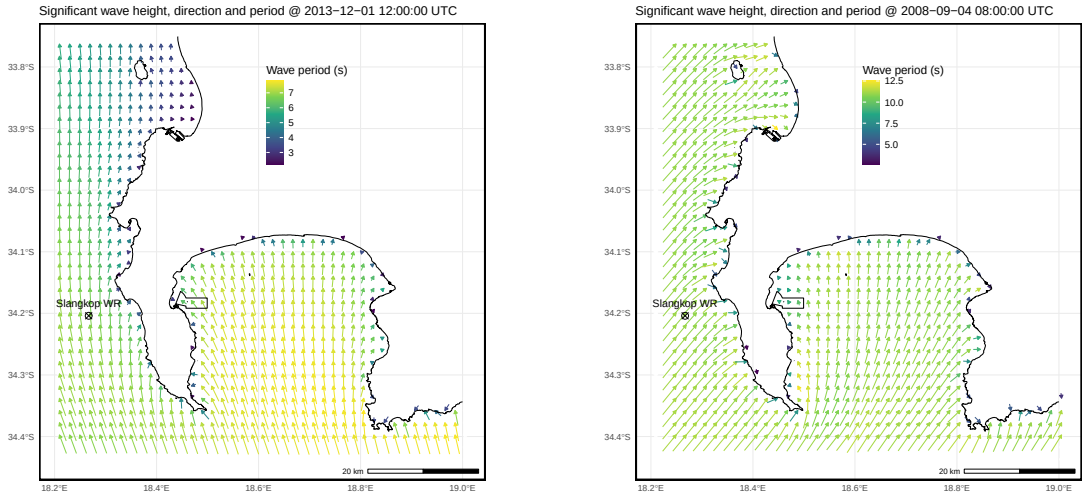

(a) Southerly swell - 2013-12-01 12:00 UTC

(b) Southwesterly swell - 2008-09-04 08:00

Figure 5. Modelled wave heights in False Bay illustrating the shielding effect of the Cape Peninsula on southwesterly swells. The study area is exposed to southerly swells. SWAN model outputs courtesy of Christo Rautenbach and Marc de Vos.

2.6. Surface and bottom currents

Atkins (1970*b*) found wind-driven surface currents dominate False Bay. He describes a clockwise circulation driven by SE winds and an anti-clockwise circulation driven by NW winds. Current meters show that surface water is driven into the middle of the bay by SE winds and exits on the eastern and western sides (Grundlingh and Largier, 1991; Wainman et al., 1987).

Circulation models indicate complicated surface-current patterns for different wind speeds and wind directions (Jury, 2020; Vos et al., 2021). Bottom currents tend to flow differently from surface currents (Coleman et al., 2021; Vos et al., 2021). The models show that in the study area, surface and bottom currents move in a northerly direction with SE winds. With NW winds, surface currents move in a southerly direction. In contrast, bottom currents move in the opposite direction (Coleman et al., 2021). In other words, wind-driven bottom currents flow northwards through the study area, no matter how the wind blows. Tide-driven currents develop when there is no wind-forcing and flow northward during incoming tides and southward during outgoing tides (Vos et al.,

(a) Shirley-T

(b) Annie-K

Figure 6. Catamaran workboats used for data collection

2021).

3. Methods

3.1. Data collection

Data collection occurred in two stages during 1985 and 1986. The initial phase involved seafloor mapping using side-scan sonar and echosounder, followed by sediment sampling and diver inspections for verification in the second phase. This was conducted using two catamaran workboats, the Shirley-T and Annie-K (Figure 6), equipped for surveying and diving.

3.1.1. Geophysical survey

An integrated survey system, comprising an autopilot, single-beam echosounder, and an analogue side-scan sonar system, steered a small catamaran boat along predetermined tracks. A microwave ranging system provided one-meter accuracy position fixes (the

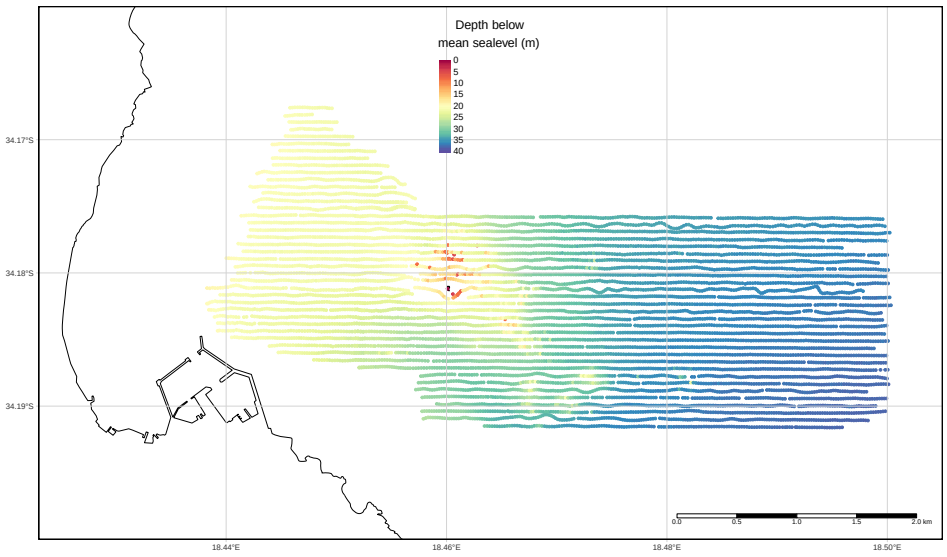

Figure 7. Depth soundings along 66 east-west oriented survey tracks

survey was conducted before GPS became prevalent). The survey unfolded in two phases: The first phase recorded 7811 depth soundings at one-second intervals along 66 east-west tracks spaced 60m apart (Figure 7). The second phase collected 10.8km^2 of 100kHz side-scan sonar imagery along 22 east-west tracks spaced 180m apart (Figure 12). Tracks were traversed at 3.5 knots to achieve a 2m along-track resolution. The system produced side-scan sonar imagery, corrected for speed and slant range, at a 1:1000 scale, with position fixes marked every 30 seconds on the paper records.

3.1.2. Sediments sampling and diver-inspections

Proper interpretation of side-scan sonar imagery requires quality ground control (Bouma and Rappeport, 1984). To avoid misinterpretation of the side-scan sonar imagery, sediment samples and information from SCUBA diver inspections were obtained from several locations within the study area.

This study collected 71 sediment samples: 66 were obtained using a hand-operated Van Veen grab (Van Veen, 1936), and SCUBA divers collected five during seafloor inspections. The sampling sites targeted different patterns of acoustic reflectivity (acoustic facies) observed on the side-scan sonar imagery. Figure 8 shows the location of each sample site. The Van Veen grab retrieved up to 0.6 litres of sediment. Retrieved samples were

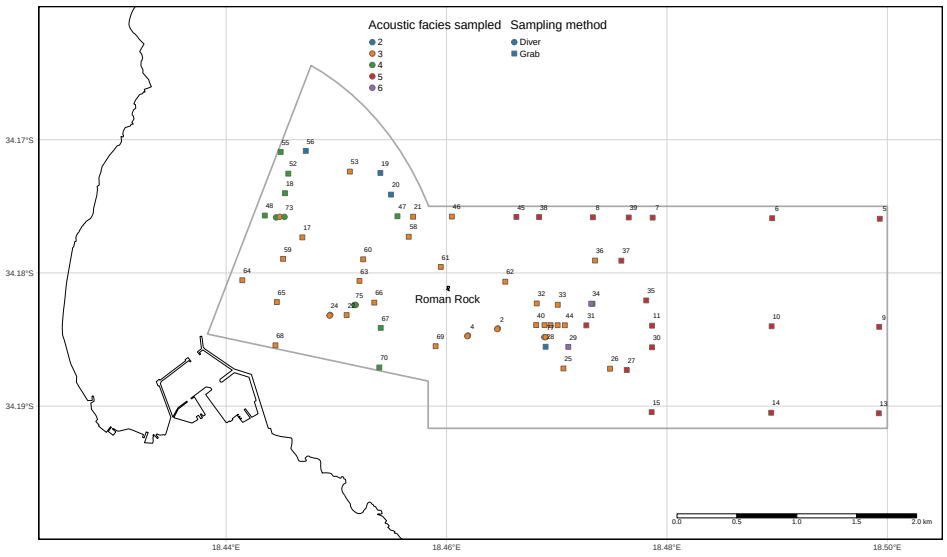

Figure 8. Sediment sample sites. Colours indicate which acoustic facies were sampled. Shapes indicate the sampling method used.

emptied into a bucket to allow fines to settle and remove macrofauna and excess water before being transferred into a labelled 700 ml jar. Diver-collected samples were scooped into similar jars and capped underwater before being brought to the surface.

The SCUBA divers inspected different patterns of acoustic reflectivity at ten dive sites (Figure 9). Ten divers, including three marine geologists and one marine biologist, participated. For safety, dives were limited to fair weather and depths under 30 metres, restricting sites to the study area's shallower western part. Sediment samples were collected at six dive sites. Divers recorded notes on plastic sheets and took underwater photographs with Nikonos IV A cameras.

3.2. Data processing and analysis

3.2.1. Geophysical survey

The 1:1,000 scale paper imagery was reduced to 1:2,000 scale using a photocopier for easier handling. These reduced copies were arranged in a mosaic on the lab floor, allowing the first author to visually assess and classify sonograph facies based on acoustic reflectivity, following the approach of Kidd, Simm and Searle (1985). Underwater Surveys then transferred these facies onto 1:2,000 scale track charts, which were photographically

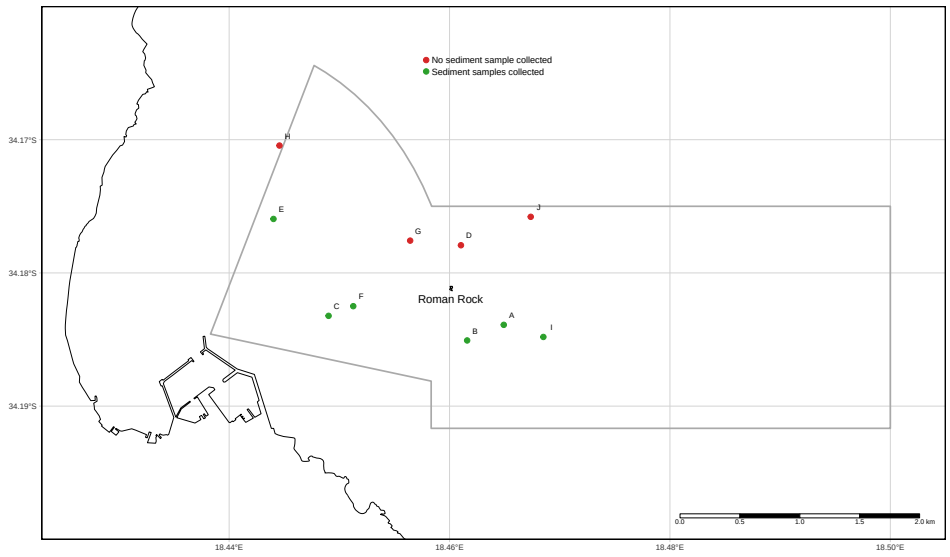

Figure 9. SCUBA dive sites. All the dive sites are in water less than 30m deep. Sediment samples were collected at six of the dive sites.

reduced to 1:10,000 scale and compiled into a single map. This map was digitised as an ESRI shapefile for integration with other spatial data. While digital methods offer precision and efficiency, physically assembling the mosaic at a 1:2,000 scale provided an unequalled overview, enabling pattern recognition and spatial interpretation in a way often lost on a computer screen.

The 7811 depth soundings, time-stamped and tide-corrected, were converted into XYZ data points. One-meter interval depth contours were generated from these data using TNTmips software and saved as an ESRI shapefile.

3.3. Sediment sample analysis

The workflow used to determine the textural and compositional properties of all the sediment samples is presented in Figure 10.

3.3.1. Sample preparation

The wet sample was split by “coning and quartering” (Gerlach, Dobb, Raab and Nocerino, 2002). A quarter was put aside for laboratory analysis. This sub-sample underwent desalination via osmosis in dialysis tubing immersed in refreshed tap water overnight. The desalinated sample was then split again, allocating three-quarters for

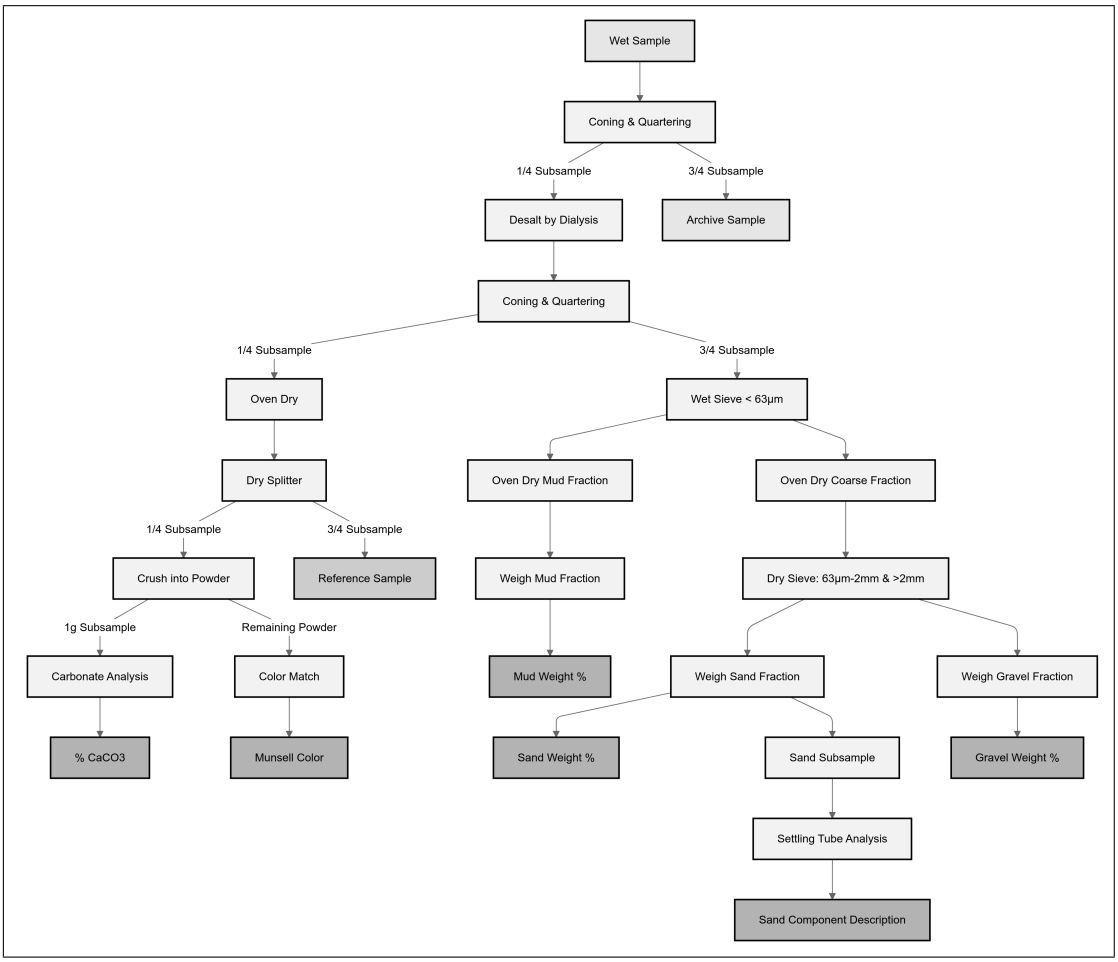

Figure 10. Sediment sample analysis workflow

texture analysis and the remaining quarter for composition analysis.

3.3.2. Sieving

The desalinated texture split was wet-sieved through a 63μm screen, separating the mud (less than 63μm) from the coarser fraction. The mud was allowed to settle in plastic tubs, decanted, and then dried in glass beakers at 100 °C for 24 hours for weighing. The coarse fraction underwent similar drying, followed by a 5-minute mechanical sieve through 63μm and 2mm screens to separate gravel, sand, and pan-mud – the latter being silt retained on the 63μm screen due to water surface tension. After weighing, pan-mud was added to the wet-sieved mud weight for total mud weight calculation. The gravel, sand, and mud proportions were then calculated as percentages of the total dry weight.

3.3.3. Sand size-analysis

For settling-tube analysis, less than 10g of the sand fraction was sub-sampled using a dry sample splitter. Equipment issues meant samples had to be analysed using the Council for Geoscience and the University of Cape Town settling tubes. These shared the same basic hardware configuration and microcomputer setup – the software for performing rapid and precise statistical analysis of sand-size distribution was essentially identical (Brink and Rogers, 1985; Flemming and Thum, 1978).

3.3.4. Calcium carbonate analysis

The desalinated composition-split was oven-dried and then split again. One quarter was crushed into a fine powder with the remaining three-quarters used as a reference sample for the sonograph interpretation. Each crushed sub-sample was colour-coded using Munsell (1975) soil-color charts before being analyzed for $CaCO_3$ using the "Karbonat Bombe" method (Birch, 1981; Müller and Gastner, 1971).

Five millilitres of concentrated hydrochloric acid (HCl) was added to 1g of the crushed sample in an airtight container fitted with a pressure gauge. The pressure of the released gas was normalised against a standard for pure $CaCO_3$, giving the percentage $CaCO_3$ for the sample. Standards were determined every five samples as this method is sensitive to air temperature and atmospheric pressure variations.

3.4. Megascopic description of components

The gravel and sand fraction components were examined using a procedure based on the Ingram (1965) method. The gravel fraction was inspected visually, while the sand fraction was examined under a binocular microscope. Each sample's components were identified, and their relative abundances were categorised as 'dominant' (>50%), 'major' (5-50%), 'minor' (1-5%), or 'trace' (> 1%). Identification of specific biogenic components required consultation with marine biologists.

4. Observations

4.1. Bathymetry

An NW-SE oriented reef divides the study area into two, as shown in Figure 11. This reef, around two kilometres long and one kilometre wide, features several steep granite pinnacles rising 2 m to 20 m above a smooth seafloor. Notably, three pinnacles pose navigational hazards: Roman Rock, marked by a lighthouse; Castor Rock, shallowest at about three meters; and Rambler Rock, with a minimum depth of eight meters. To the northwest, the seafloor is flat and 20-22 m deep, whereas to the southeast, it forms a narrow trough, less than a kilometre wide and up to 33 meters deep, between the reef and coast. East of the reef, the seafloor gradually deepens from 25 m to 38 m towards the southeast corner of the area, with a slight channel-like depression observed northwest of Roman Rock.

4.2. Side-scan sonar survey

Equipment issues and the need to navigate around shallow and exposed reefs meant that only 90% of the study area was surveyed by side-scan sonar (10.8 km^2). Six patterns of acoustic reflectivity (acoustic facies) were identified on the side-scan sonar imagery (Figure 12). The characteristic features of the six acoustic facies are detailed in Table 1. Facies 1 corresponds to rocky areas in Figure 11. Facies 2 to 6 occur in areas with little relief.

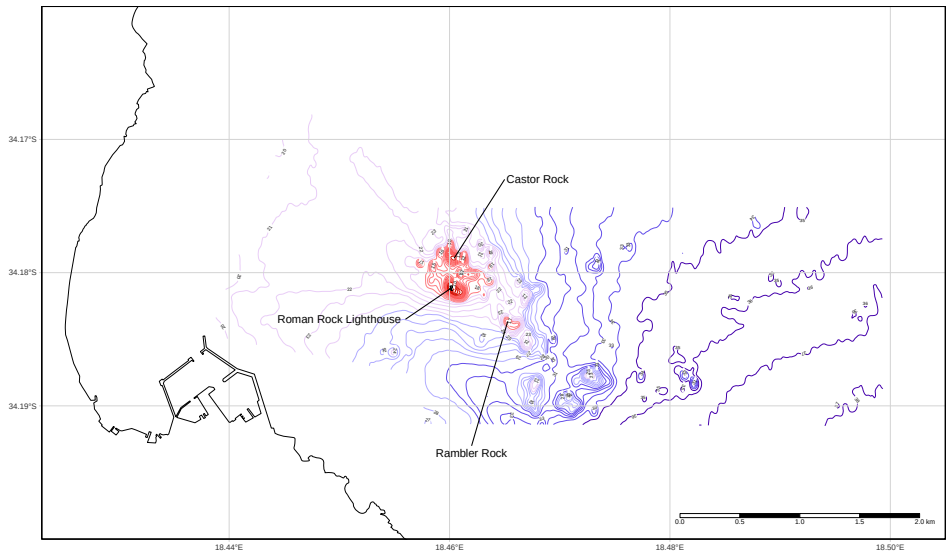

Figure 11. Bathymetry of the study area (one-meter contour-interval). A NW-SE reef bisects the study area.

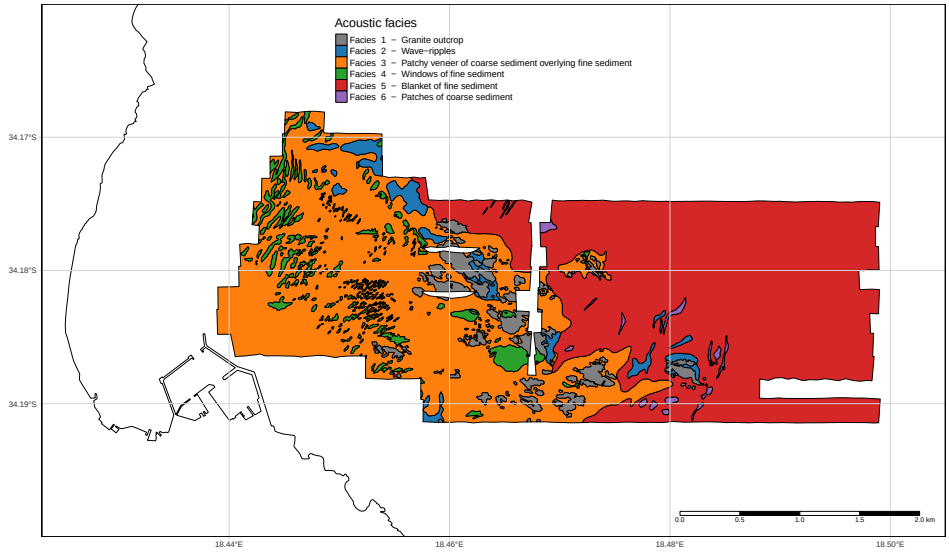

Figure 12. Acoustic facies map of the study area

.

Table 1.

Facies	Relief	Acoustic Reflectivity	Sonograph Pattern	Sediment Texture	SCUBA Diver Observations	Interpretation
1	Rugged	Strong	Lineaments within an irregular blocky pattern of light and granite outcrops west of the study area. dark tones.	–	Granite outcrop, similar to the coastal granite outcrops west of the study area. Outcrops are covered with marine organisms. The base of the outcrops is surrounded by bioclastic debris.	Cape Peninsula Granite.
2	Low	Moderate	Alternating bands of light and dark tones oriented ENE-WSW and space about one meter apart.	Sand, gravelly sand, and gravel	Straight-crested bifurcating ripples with a wavelength between 0.8m to 1.2m and amplitude between 0.2m and 0.3m, ENE-WSW crest orientation.	Large-scale, long-crested trochoidal wave ripples.
3	None	Moderate to weak	Uneven featureless medium-gray tone	Sand and gravelly sand	Small (1 to 2 meter wide) patches of gravelly calcareous sediment overlying relict quartzose fine to medium sand. Ophiuroids and crinoids are common.	Patchy veneer of calcareous gravelly sediment overlying a quartzose fine to medium sand.
4	None	Weak	"Cloud-like" and "tongue-like" patches of light tone	Sand	Rippled fine to medium sand-patches. Ripples are straight-crested, symmetrical, and bifurcate. Ripples have a wavelength between 10cm and 20cm and an amplitude of 1cm to 3cm. ENE-WSW crest-orientation. Apart from some pinnid bivalves, the patches are barren.	Blanket of quartzose fine to medium sand.
5	None	Weak	Slightly speckled, featureless light tone	Sand	Rippled quartzose fine to medium sand. Ripples are straight-crested, symmetrical, and bifurcate. Ripples have a wavelength between 10cm and 20cm and amplitude ranging from 1cm to 3cm. ENE-WSW crest-orientation. Few ophiuroids and asteroids are present.	Windows of quartzose fine to medium sand.
6	None	Moderate	Patches of medium-gray tone	Sand	None.	Coarse sediment patches?

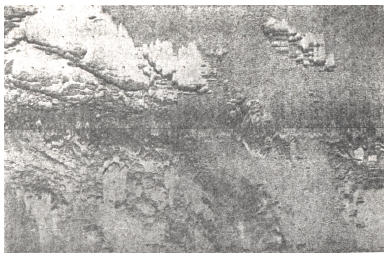

(a) Facies 1 – Cape Peninsula Granite and Facies 2 – Wave ripples

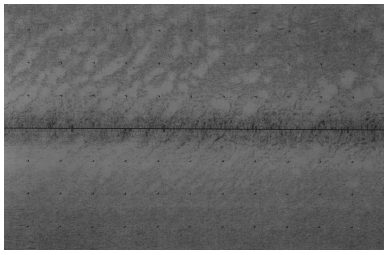

(b) Facies 4 – Cloud-like patches of fine to medium sand.

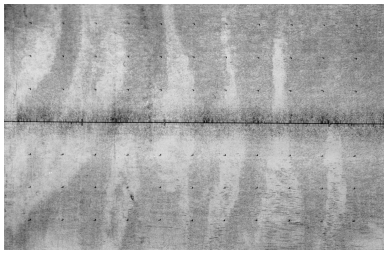

(c) Facies 4 – Tongue-like patches of fine to medium sand.

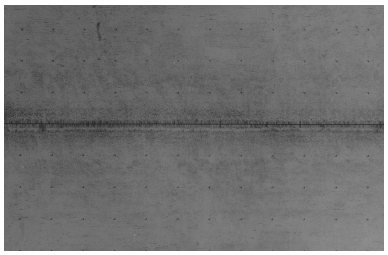

(d) Facies 4 – Cloud-like patches of fine to medium sand.

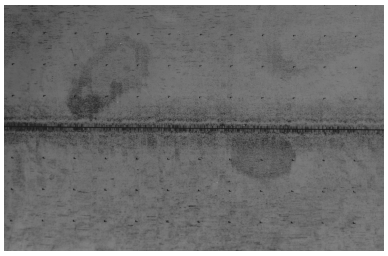

(e) Facies 6 – Coarse sediment patches within Facies 5?

Figure 13. Example sonograms. Internal tick-marks are at 25m intervals.

4.2.1. Facies 1

Figure 12 shows the distribution of Facies 1, which coincides with known reefs plotted on official nautical charts (SA Navy Nautical Chart 1017 and British Admiralty Nautical Chart 1922). The lineaments seen in Facies 1 follow several directions, but the best-defined lineaments trend WNW-ESE, parallel to the principal joint direction in the granite outcrops onshore (Boocock, 1951; Theron, 1984). Divers at Rambler Rock and near Roman Rock observed large, well-jointed, rounded granite boulders (as tall as 5m) resting on a larger rocky base (massif) or protruding above the sediment. The outcrops provide a solid substrate for both calcareous and soft-bodied marine organisms and are surrounded by bioclastic debris.

4.2.2. Facies 2

Facies 2 occurs adjacent to, or immediately north of, Facies 1, between 20 m and 35 m water depth (Figure 12). A diver inspection near Roman Rock revealed that Facies 2 consisted of large-scale sedimentary bedforms. The bedforms, spaced 0.8 m to 1.2 m apart and 0.2 m to 0.3 m high, were symmetrical with long and straight crests that were sometimes bifurcated in a crest-parallel direction (Figure 14). The crests had the same ENE-WSW orientation as the light and dark bands on the side-scan sonar imagery. The 0.8 m to 1.2 m bedform wavelength is near the 0.25 m (across-track) and the 2.09 m (along-track) resolution limits of the side-scan sonar system and thus not easy to distinguish on the side-scan sonar imagery. The bed forms were developed in calcareous gravel and sand with coarser sediment in the troughs and finer sediment on the crests.

4.2.3. Facies 3

Facies 3 occurs in the western half of the study area, at depths between 20 m and 35 m (Figure 12). Sediment samples from Facies 3 range from quartzose sand to calcareous gravel. The samples nearest the granite pinnacles are usually composed of shell debris such as cirripede (barnacle) and mollusc fragments. In contrast, the samples farther away from the rock pinnacles, between Roman Rock and the Simon's Town harbour wall, are composed of a mixture of coralline-algal fragments and quartzose sand. Dive sites C, E, F, and H (Figure 9) revealed both living and dead unattached coralline algae (subfamily

Melobesioideae) forming autochthonous structures, referred to as 'maerls' or 'marls' (e.g Bosence, 1976; Steneck, 1986), which create a complex habitat supporting diverse taxa (Steller, Riosmena-Rodriguez, Foster and Roberts, 2003). These maerl structures, a few meters across and centimetres high, often appear as elongated strips oriented ENE-WSW over quartzose sand and are associated with crinoids and brittle stars. Additionally, divers observed pebble-sized quartz and feldspar fragments and Venus verrucosa shell fragments on the seafloor in Facies 3.

4.3. Sedimentology

4.3.1. Sediment texture

Figure 15 shows that the sediment samples collected in this study are either gravelly sands or sandy gravels. The samples are essentially mud-free. Figure 16 presents a breakdown of sediment texture by Acoustic Facies. Facies 3 exhibits the most variation in sediment texture, ranging from slightly gravelly sand to gravel. Most of the samples from the other acoustic facies are slightly gravelly to gravelly sands. Figure 17 shows a clear relationship between sediment texture and sediment composition: the higher the gravel fraction, the more calcareous the sediment is. The following section presents the analysis of sediment composition, which clearly shows that the gravel fraction consists primarily of bioclastic components.

4.3.2. Sediment composition

Results from the visual examination of gravel components and binocular examination of sand components are presented in Figures 22 and 23, respectively. These show the abundance of each component for all the samples from each facies. Abundances are expressed in terms of Ingram (1965) categories. Mollusc and coralline algal fragments dominate the gravel fraction in all the sediment samples.

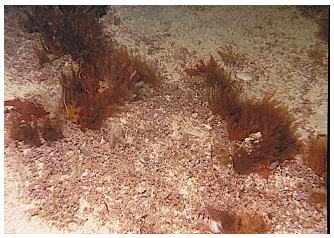

(a) Unattached branching coralline algae (maerl) together with dark-coloured feather stars (*Comanthus wahlbergi*) at Dive Site F (Facies 3). The field of view is approximately one metre.

(b) Isolated granite boulder in the middle of a wave-ripple field at Dive Site D (Facies 2).

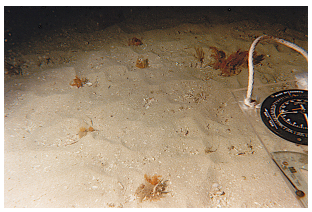

(c) Fine to medium quartzose sand in Facies 4 cloud-like pattern at Dive Site H.

(d) Small-scale ripples in fine to medium quartzose sand at Dive Site J (Facies 5). Note the ophiuroids (brittle stars) in the foreground.

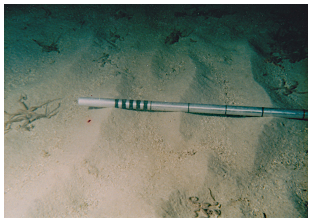

(e) Rippled quartzose fine to medium sand in cloud-like patches at Dive Site H (Facies 4). The measuring staff is marked at 1 cm and 10 cm intervals. Note the slightly coarser material in the troughs.

Figure 14. Underwater photographs from in-situ diver inspections. Refer to Figure 9 for dive site locations.

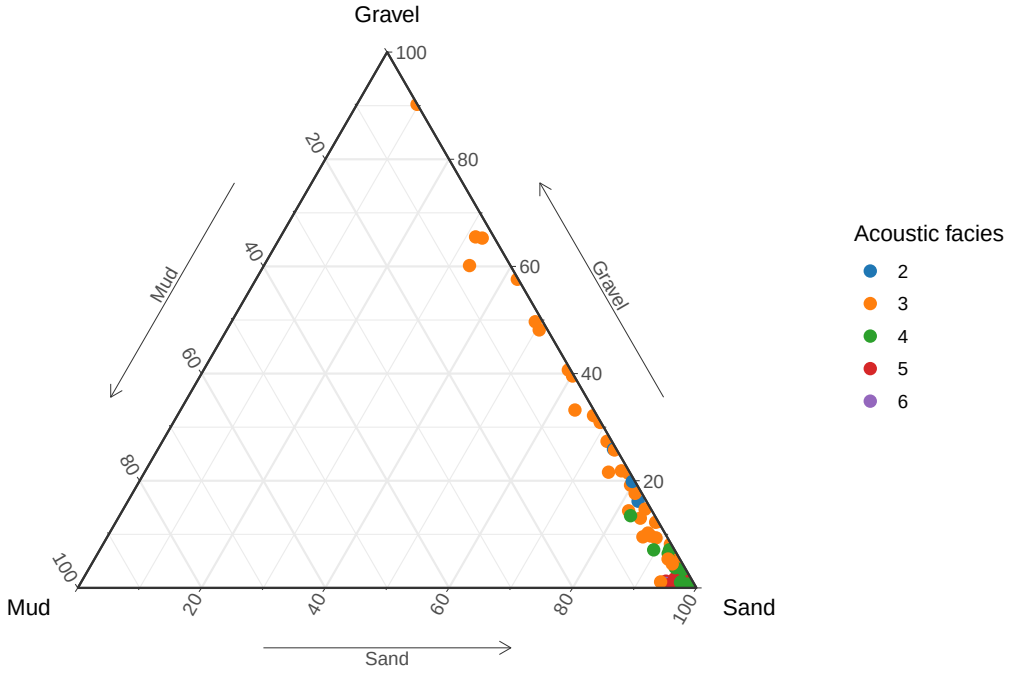

Figure 15. Gravel-Sand-Mud ternary diagram. The sediment is largely mud-free. Samples collected in Facies 3 range from gravelly sand to gravel. Most of the samples from the other acoustic facies are slightly gravelly to gravelly sands.

5. Interpretation

This section interprets the geological significance of the side-scan sonar, echosounder, sediment sample data and diver observations.

5.1. Facies 1 - Cape Peninsula Granite

The pattern of reflectivity produced by the exposed Cape Peninsula Granite (Facies 1) has been observed elsewhere in False Bay and further afield in Table Bay (MacHutchon, de Beer, Van Zyl and Cawthra, 2020; Woodborne and Flemming, 2021) and Saldhana Bay (De La Cruz, 1978) and is typical of granite. The WNW-ESE lineaments seen on the side-scan sonar imagery collected in this study correspond to the principal joint direction in the Cape Peninsula Granite observed along the Simon's Town coast (Boocock, 1951; Theron, 1984). The granite outcrops observed in the side-scan sonar imagery may be

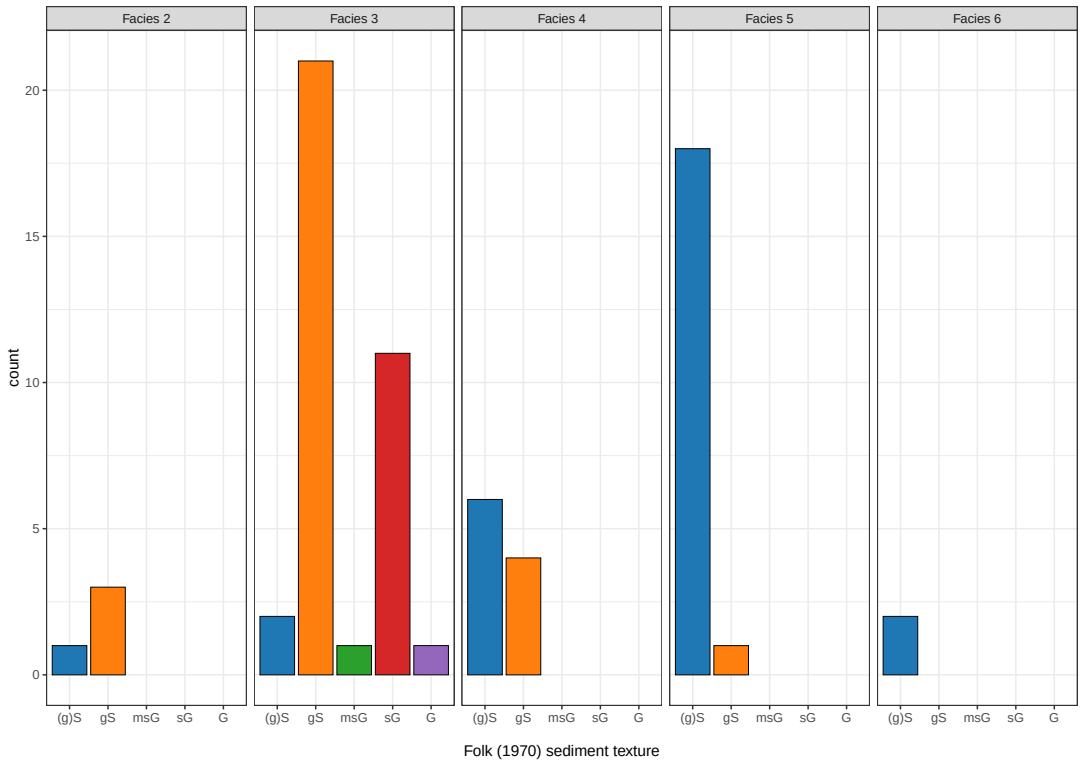

Figure 16. Breakdown of sediment texture per facies.
(g)S = slightly gravelly Sand, gS = gravelly Sand, msG = muddy sandy Gravel, sG = sandy Gravel, G = Gravel.

described as submerged tors where the joints in the granite are more widely spaced (Du Plessis and Glass, 1991; Glass, 1977; Linton, 1955).

5.2. Facies 2 - Wave Ripples

The underwater photographs at dive site D (Figure 9) verify that Facies 2 represents rippled calcareous gravel1y sand or sand. This pattern of reflectivity has been observed elsewhere along the South African coast, for example, in Saldhana Bay and off Namaqualand (De La Cruz, 1978; Flemming, 2019).

The symmetry, WSW-ENE orientation, and crest length of the ripples suggest that orbital currents generated by SSE swells form them and, therefore, should be more accurately defined as long-crested trochoidal wave—ripples (Reineck and Singh, 1980). The wave ripples are located near or to the north of granite reefs. This implies that the orbital currents forming these ripples are intensified when waves from the SSE pass

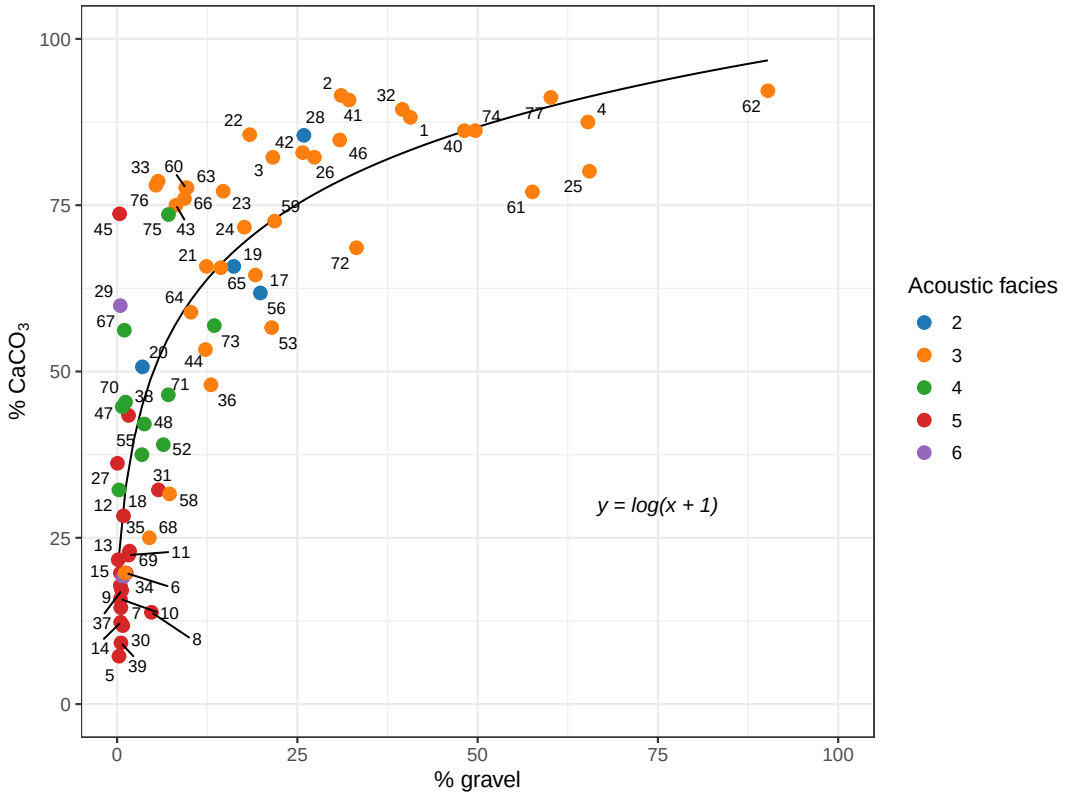

Figure 17. Percent gravel versus percent $CaCO_3$. The calcareous fraction increases exponentially with an increasing gravel fraction.

north-westwards over reefs. The shallow seafloor depression observed to the NW of Roman Rock (see Figure 11 – bathymetry map) is likely to have been generated by stronger bottom currents. The sediment where the wave ripples occur has a mean size of 0.56mm (coarse sand). Figure 24 suggests that the minimum orbital current velocity (μ_m) needed to move sediment of this size is approximately 0.25 to 0.3 ms^{-1}.

Substituting an arbitrary wave-period of 10 s (within the 8 s to 14 s range described by Shipley (1964)), a value for u_m of 0.3 ms^{-1} and a depth (h) of either 20 m or 35 m (the depth—range of the wave ripples) into equation 1 (Komar and Miller, 1973), the minimum wave-heights (H) needed for wave ripple formation are 0.9 m and 1.8 m at depths of 20 m and 35 m, respectively.

$$\mu_m = \frac{\pi H}{T sinh(2\pi h/L)} \tag{1}$$

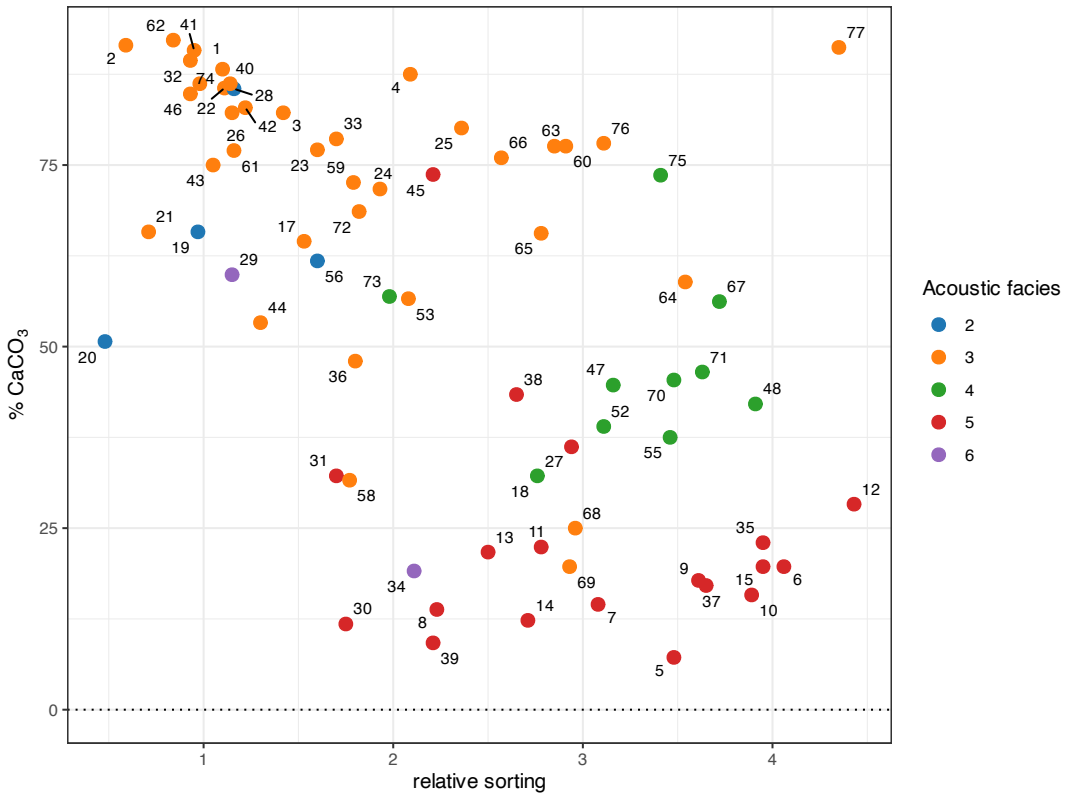

Figure 18. Relative sorting versus $CaCO_3$. Facies 3 calcareous sands are better sorted than Facies 5 quartzose sands.

where μ_m is the threshold orbital velocity (ms^{-1}), H is the wave-height (m), T is the wave period (s), L is the derived wave-length (m) where $L = 1.56T^2$, h is the water depth (m).

Note that Komar and Miller's 1973 equation is based on empirical studies addressing the entrainment of spherical quartz grains. Irregularly shaped bioclastic components most likely require higher orbital velocities (i.e. higher wave heights) to move (Li, Yu, Gao and Flemming, 2020).

The wave ripples were inactive when inspected by divers during fair-weather conditions. This, together with the 0.9 m to 1.8 m range of minimum wave heights required to generate μ_m and the quiet-water epifaunal assemblage found in the study area, suggests that wave ripple formation is likely to only occur during prolonged summer southeasterly gales when the highest waves occur in False Bay (Theron and Schoonees, 2007).

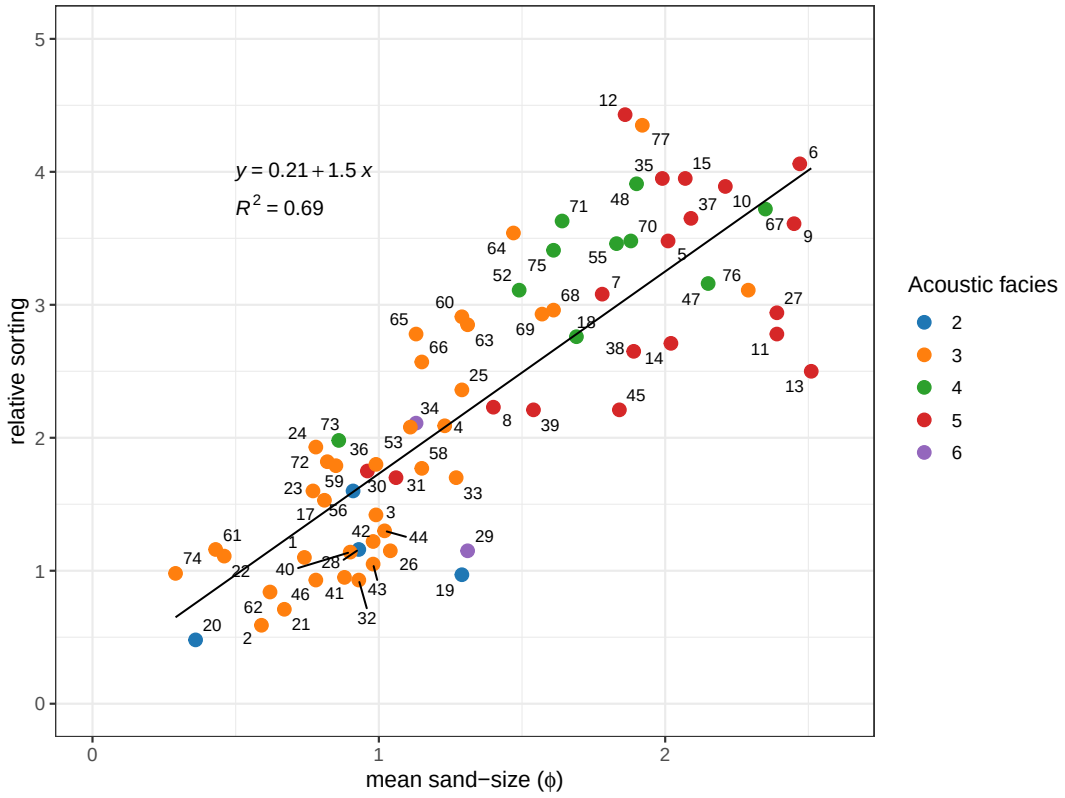

Figure 19. Mean sand-size versus relative sand-sorting. Sand becomes less well-sorted as it becomes finer-grained.

5.3. Facies 3 - Patchy Veneer of Calcareous Sediment

Facies 3 represents a patchy veneer of calcareous gravel or gravelly sand overlying fine to medium quartzose sand. The patchiness of the calcareous sediment is attributed to many environmental factors, such as the nature of bottom—currents, type of substrate, predation, and food—supply, that affect the distribution of $CaCO_3$ secreting organisms. Maerl is present in almost every coastal ecosystem around the world (Foster, 2001). It comprises broken fragments from larger fructose forms of coralline algae growing on rocks. The fragments continue to grow unattached on the seafloor after they have broken off (Johansen, 2018; Woelkerling, Irvine and Harvey, 1993). The concentration of detritus-feeding ophiuroids on top of the maerl may be because some entrained detritus becomes trapped in the interlocking branches of coralline algae as the water filters through them.

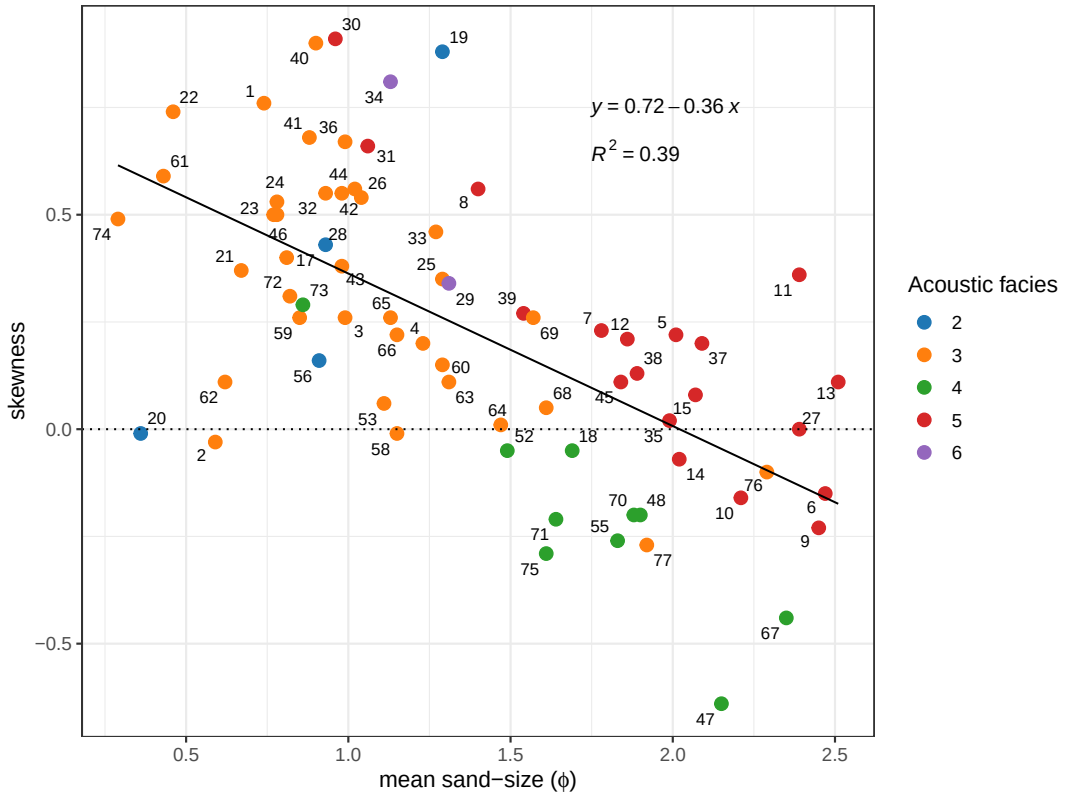

Figure 20. Mean sand-size versus skewness. Sand becomes less positively skewed as it becomes finer-grained.

5.4. Facies 4 - Windows of Calcareous Fine to Medium Sand

The reflective pattern distinguishing Facies 4 from Facies 3 is produced by large patches of rippled, calcareous, fine to medium quartzose sand. Facies 4 appears to represent gaps in the veneer of calcareous gravelly sediment, large enough for side—scan sonar to detect the underlying fine to medium quartzose sand. In contrast, in Facies 3, the much smaller windows of fine to medium quartzose sand in the veneer of calcareous sediment are too small to be resolved by side—scan sonar. This interpretation is based on evidence provided by underwater photographs taken by divers at dive sites G and H (Figures 9 and 14).

The WSW-ENE orientation of the "cloud-like" sand patches may be due to winnowing by orbital currents generated by SSE waves, whereas the "tongue-like" patches are possibly produced by a predominant northward-moving bottom-current (Atkins, 1970*b*; Vos et al., 2021). The WSW-ENE crest orientation and bifurcated ripples seen by divers within Facies 4 at dive sites F and H (Figures 9 and 14) suggest that these are also a

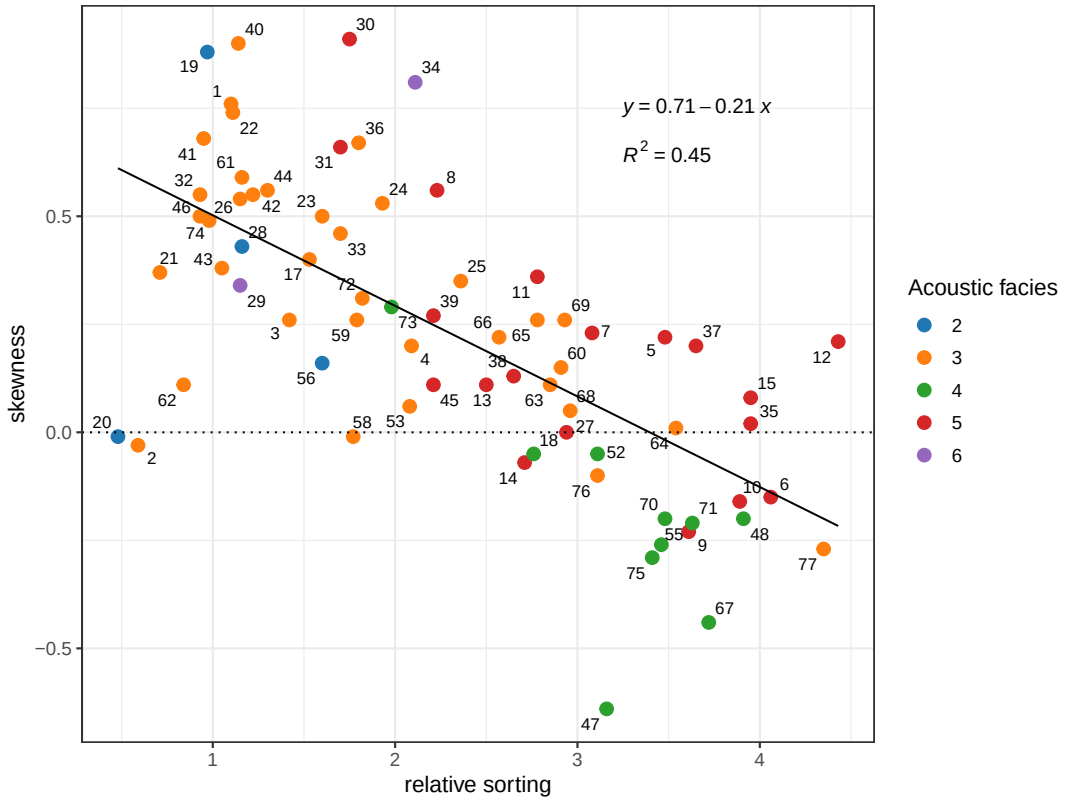

Figure 21. Relative sorting versus skewness. Sands become more positively skewed as they become more well-sorted.

product of SSE wave-generated orbital currents.

5.5. Facies 5 - Blanket of slightly calcareous fine to medium sand

Facies 5 is produced by an extensive blanket of slightly calcareous, fine to medium quartzose sand. The speckled areas seen on the sonographs in Facies 5 (Figure 13) are attributed to small wave ripples and epifauna that cannot be resolved by side-scan sonar. This interpretation is verified by underwater photographs of small-scale ripples and epifauna taken at dive site J (Figure 9 and 13) and by the homogeneity of the Facies 5 sediment samples. Bouma and Rappeport (1984) also found that a feature-less, even-toned seafloor may be covered with features too small or of insufficient density to be resolved by side-scan sonar. Consequently, they stress the importance of underwater photography in verifying the interpretation of side-scan sonar imagery. This project confirms the value of this approach, particularly regarding Facies 3 to 5.

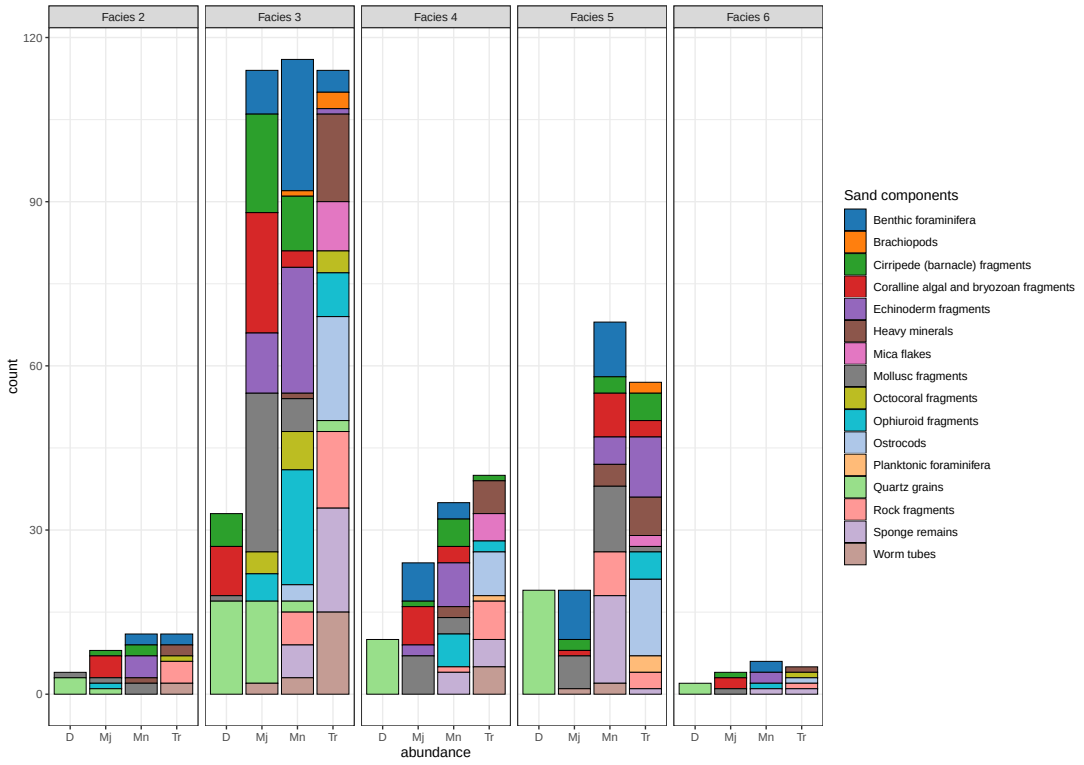

Figure 22. Breakdown of sand components.
D = Dominant (> 50%), Mj = Major (5% - 50%), Mn = Minor (1% - 5%), Tr = Trace (< 1%)

The WSW-ENE crest orientation and bifurcation of the small-scale ripples seen in Facies 5 at dive site J imply that SSE wave—generated orbital currents produce these.

5.6. Facies 6 - Coarse sediment patches

Any interpretation of Facies 6 is hampered by the lack of underwater photographs, diver—observations, and sufficient sediment samples. The two sediment samples from Facies 6, a medium quartzose sand and a medium calcareous sand, suggest that Facies 6 represents medium sand. The rounded Facies 6 patches depicted in Figure 13 may represent exposed saprolite.

5.7. Modern subtidal energy regime

Data from the ADCP deployed off Miller's Point, and the output of circulation models show that bottom currents in the study area are generally weak, seldom exceeding 0.2 $ms^{-}1$ (Coleman et al., 2021). The observed epifaunal assemblage confirms that

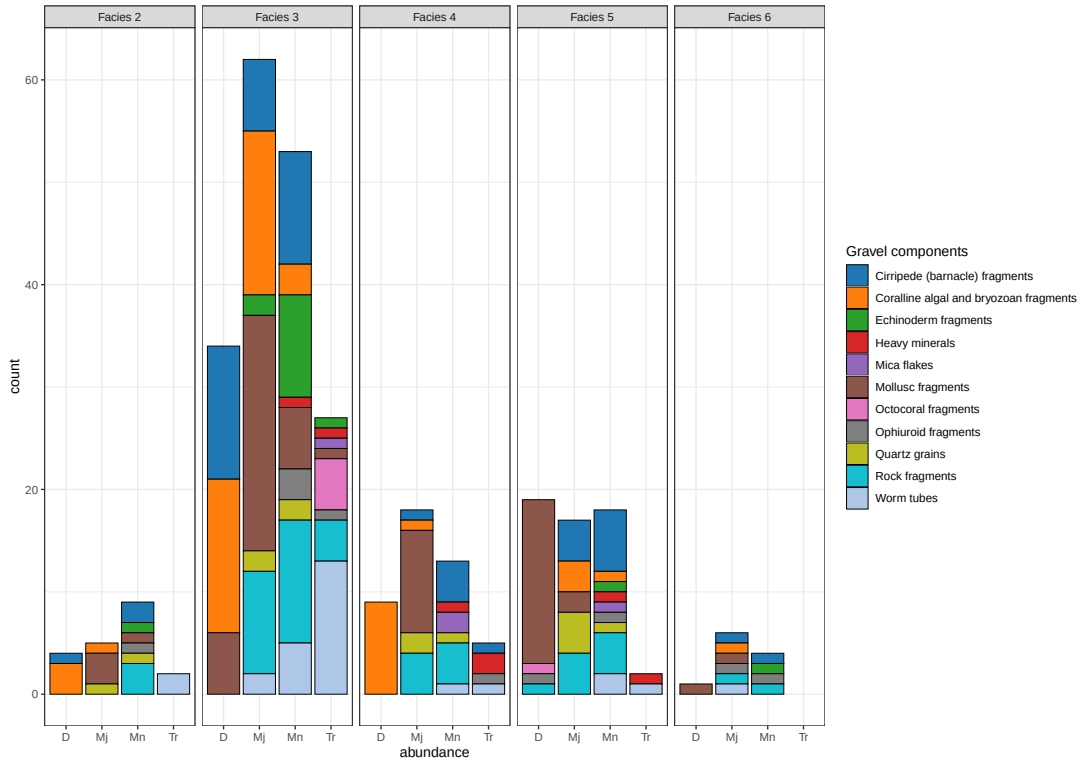

Figure 23. Breakdown of gravel components.
D = Dominant (> 50%), Mj = Major (5% - 50%), Mn = Minor (1% - 5%), Tr = Trace (< 1%)

the study area is a low-energy environment. The delicate filter-feeding pinnid bivalve Atrina squamifera observed in Facies 4 typically occurs in fine sediment in a sheltered environment where it is least susceptible to breakage or burial (Day, 1969, p. 143) (Kilburn and Rippey, 1982, p. 167). The same applies to the delicately-branched, free-living coralline—algae (maerl) which must live above the sediment in a quiet environment to survive (Steneck, 1986). The precarious attachment of the detritus-feeding crinoid, Comanthus wahlbergi, to the loose maerl and the vertically semi-embedded pinnid bivalves, indicates that bottom currents must be weak. The density of ophiuroids observed in Facies 3 is also indicative of a low-energy environment, according to Branch and Branch (1981, p. 238) who comment: “brittle stars are often gregarious and in deeper, calmer, waters dense assemblages may be found”.

Another indication that the subtidal zone is a low-energy environment is from a side-scan sonar survey conducted three years earlier of an area overlapping the present study area (Russell-Cargill, 1983). A comparison of the side-scan sonar imagery from the

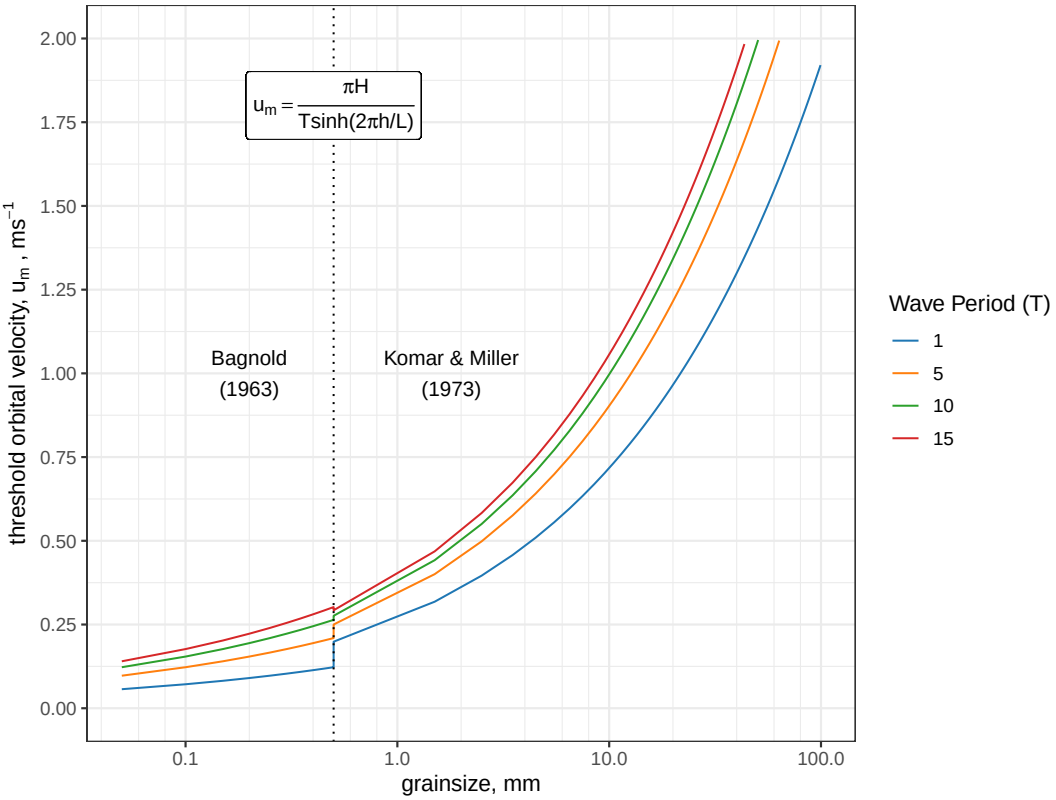

Figure 24. Near-bottom orbital velocity u_m for sediment threshold under waves. Plot generated using computational routines described in Komar and Miller (1975). For sediment grain sizes < 0.5mm, the curves are based on Bagnold (1963) empirical data. For grain sizes> 0.5mm, the curves are based on Komar and Miller (1973) empirical data.

previous survey and the present study shows no noticeable difference in the distribution of the different patterns of acoustic reflectivity. Thus, the modern subtidal zone in the study area is generally a stable low-energy environment, except during prolonged southeasterly gales in summer, when high-energy conditions sufficient for Facies 2 wave-ripple formation prevail. The subtle seafloor depression observed northwest of Roman Rock (Figure 11) is likely the result of wave-driven orbital currents scouring the seabed.

5.8. Sediment mixing

Flemming (1982) argues the sediment distribution in False Bay can be explained in terms of the sediment-mixing model of Folk and Ward (1957). He states: "the mixing process between two hydraulic populations of different mean sizes follows a predictable pattern revealed in the appropriate scatter plots. Progressive mixing implies that a well-sorted coarse population will initially become increasingly finer, more positively skewed and less well-sorted as the proportion of fine sediment increases. By analogy, a well-sorted fine population will become increasingly coarser, more negatively skewed and less well—sorted the greater the proportion of coarse sediment." (Flemming, 1982, p. 15).

Plotting percent $CaCO_3$ against relative sand-sorting, one sees that the quartzose sands from Facies 4 and 5 are not as well-sorted as the calcareous sediment from Facies 2 and 3 (Figure 18). Figures 19 to 21 (where mean sand size, relative sand-sorting and skewness are plotted against each other) show that the coarse relatively well-sorted sand in Facies 3 becomes less well-sorted and more positively skewed as the proportion of fine sand increases. This trend conforms to the Folk and Ward (1957) sediment—mixing model. Mixing is most apparent in Facies 3 because it has diverse end members, one a calcareous gravel and the other a moderately- to well—sorted fine to medium quartzose sand, whereas the other facies are predominantly coarse calcareous sediment or a fine to medium quartzose sand.

The degree of mixing depends on the intensity of bottom—current activity and the extent of bioturbation. The mixing of sediments in Facies 3 probably occurs because the underlying exposed fine to medium quartzose sand is more easily entrained than the overlying patchy veneer of coarse calcareous sediment. Once the bottom current

velocity decreases to a point where suspension is no longer possible, the fine to medium quartzose sand settles out on the calcareous sand and gravel. In this way, the mixing process depicted in Figures 19 to 20 is thought to occur.

5.9. Quaternary sedimentation

This section discusses the Quaternary sedimentary history of the study area, gleaned from literature on sea-level fluctuations and the probable relationship between the six sonograph facies.

During the last glacial maximum (between 26.5 and 19 ka), sea level dropped as much as 130 m below its present elevation (Clark, Dyke, Shakun, Carlson, Clark, Wohlfarth, Mitrovica, Hostetler and McCabe, 2009; Compton, Mulabisana and McMillan, 2002; Cooper, Green and Compton, 2018; Yokoyama, Lambeck, De Deckker, Johnston and Fifield, 2000). The Cape Flats would then have extended beyond the present-day entrance to False Bay. Apart from the granite pinnacles, the study area would have formed part of an extensive aeolian dune field deposited on the newly exposed floor of False Bay (Bowie, 1966). Parts of the area would probably also be covered by sandstone debris (talus) deposited by mass wasting along the steep flanks of the Swartberg mountain (Rogers, 2018). During the subsequent Flandrian transgression, these Late Pleistocene sediments were probably eroded and redistributed by wave action as the sea transgressed across the study area.

This process persists today at Swartklip on the northern shore of False Bay. Here, a 50 m thick succession of Late Pleistocene sands is being eroded and redistributed by wave action (Flemming, 1982). Barwis and Tankard (1983) recognise four depositional facies in the Swartklip succession. From the base up, these are beach, estuarine, washover—fan, and aeolian facies (i.e. a Late Pleistocene regressive sequence). The aeolian sediment seen at Swartklip and in boreholes north of Swartklip, consists of cross-bedded, slightly calcareous, moderately- to well-sorted fine to medium quartzose sand (Hay, 1981). As the quartzose sand found in the study area has textural properties similar to those found at Swartklip, it is concluded that it is also derived from aeolian deposits that were reworked by waves during the Flandrian transgression. In other words, the quartzose sand found in the study area is a relict of both an aeolian and a shoreline environment

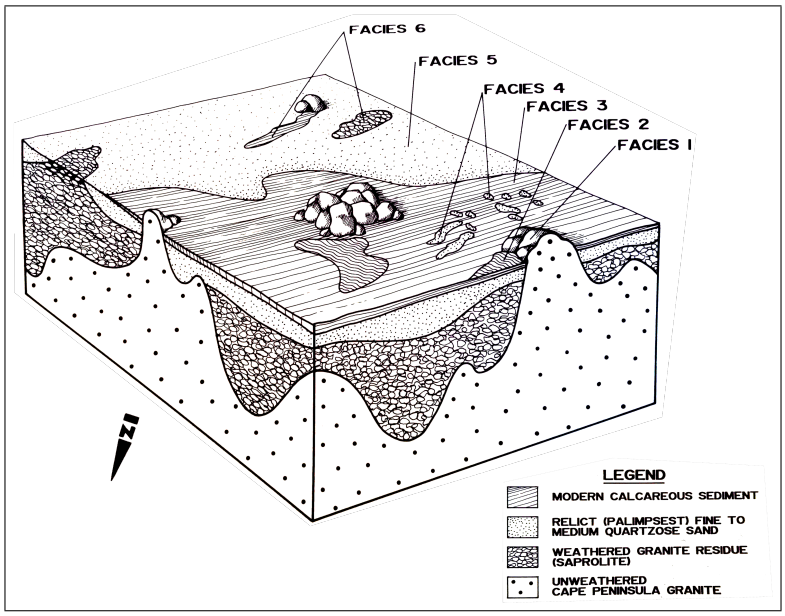

Figure 25. Sketch showing the probable geological relationship between the six acoustic facies.

but presently lies in a modern low-energy subtidal environment episodically affected by southeasterly gales in summer. Therefore, it is not only "relict" but also "palimpsest" (McManus, 1975). Palimpsest sediment has the petrographic attributes of an earlier and later (in this instance, modern) sedimentary environment (Swift, Stanley and Curray, 1971).

Towards the end of the Flandrian transgression, the study area would have become fully submerged, marking the onset of the modern sedimentary environment in which calcareous sediment derived from molluscs, cirripedes, coralline algae, and other carbonate-secreting marine organisms, started to accumulate on top of the palimpsest quartzose sand (Martins and Barboza, 2005). Figure 25 shows how the six acoustic facies are thought to relate to one another.

6. Summary and conclusions

Our side-scan sonar survey of a 12 km^2 area in the northwestern corner of False Bay revealed six distinct acoustic facies, interpreted using echosounder data, bottom samples, and SCUBA diver observations.

Facies 1 shows Cape Peninsula Granite outcrops, matching onshore patterns, with lineaments reflecting the principal WNW-ESE joint direction.

Facies 2 is marked by stationary, long-crested, trochoidal wave ripples, likely formed by currents from southeasterly gales.

Facies 3 features an uneven grey tone of calcareous gravelly sand derived from marine organisms in the shallower western areas.

Facies 4 appears as 'cloud-like' and 'tongue-like' light patches, indicating windows of underlying rippled quartzose sand.

Facies 5 is a light-toned blanket of rippled quartzose sand in deeper eastern regions.

Facies 6 consists of medium-grey patches within Facies 5, possibly representing coarse sediment, pending further confirmation.

Circulation models and epifaunal assemblages indicate that the study area is predominantly a low-energy subtidal environment, except near the reef that bisects it. Summer SSE gales likely generate strong orbital currents, driving the formation of wave ripples. Sediment analysis indicates mixing between calcareous and quartzose sediments, particularly in Facies 3. The quartzose sand is likely reworked from Late Pleistocene aeolian deposits, making the subtidal sands "relict" and "palimpsest". The deposition of calcareous sediment over this palimpsest sand marks the onset of the modern subtidal environment.

This study demonstrates the complexity of the seafloor geology off Simon's Town, underscoring the value of bottom sampling, diver observations, and underwater photography in validating sonar imagery. It also highlights the need for future research to explore sediment dynamics further, especially considering grain composition, shape, and

size and their impact on sediment movement. More comprehensive bottom-current and wave data, along with advanced hydrodynamic models, are necessary for a quantitative analysis of sediment movement.

CRediT authorship contribution statement

Andrew Terhorst: Conceptualization, Formal analysis, Investigation, Methodology, Project administration, Writing – original draft. John Rogers: Supervision, Writing – review & editing.

Declaration of competing interest

The authors declare that they have no known competing financial interests or personal relationships that could have appeared to influence the work reported in this paper.

Data availability

Interested readers can access the spatial and sedimentological data used in this study via the "Mendeley Data" open data repository at `https://data.mendeley.com/datasets/r6995krm6v/1`.

Funding

The original study was sponsored by the South African Navy (IMT projects MT-073 and OH-004) and by an M.Sc study grant from the South African Foundation for Research Development (FRD). This updated study received support from Australia's Commonwealth Scientific and Industrial Research Organisation (CSIRO).

References

Atkins, G. (1970*a*), 'Thermal structure and salinity of False Bay', *Transactions of the Royal Society of South Africa* **39**(2), 117–128.

Atkins, G. (1970*b*), 'Winds and current patterns in False Bay', *Transactions of the Royal Society of South Africa* **39**(2), 139–148.

Backeberg, N., Reid, D., Trumbull, R. and Romer, R. (2011), 'Petrogenesis of the False Bay Dyke Swarm, Cape Peninsula, South Africa: evidence for basement assimilation', *South African Journal of Geology* **114**(3-4), 335–352.

Bagnold, R. (1963), *Mechanics of marine sedimentation*, Vol. 3, Interscience, New York, N.Y., pp. 507–528.

Bang, N. (1967), 'Oceanography and a naval tragedy', *Lantern* **17**(1), 84–87.

Barwis, J. H. and Tankard, A. J. (1983), 'Pleistocene shoreline deposition and sea-level history at Swartklip, South Africa', *Journal of Sedimentary Research* **53**(4), 1281–1294.

Belcher, R. W. and Kisters, A. F. (2003), 'Lithostratigraphic correlations in the western branch of the Pan-African Saldania belt, South Africa: the Malmesbury Group revisited.', *South African Journal of Geology* **106**(4), 327–342.

Birch, G. (1981), 'The karbonat-bombe: a precise, rapid and cheap intstrument for determining calcium carbonate in sediments and rocks', *South African Journal of Geology* **84**(3), 199–203.

Boocock, C. (1951), 'The structural features and inclusions of the Cape Peninsula granite', *Transactions of the Royal Society of South Africa* **33**(2), 243–276.

Bosence, D. (1976), 'Ecological studies on two unattached coralline algae from western Ireland.', *Palaeontology* **19**(2), 365–395.

Bouma, A. and Rappeport, M. (1984), 'Verification of side-scan sonar acoustic imagery by underwater photography', *Underwater Photography* pp. 279–294.

Bowie, D. (1966), The Marine Geology of False Bay, Master's thesis, University of Cape Town.

Branch, G. and Branch, M. (1981), *The living shores of southern Africa*, Struik Publishers.

Brink, V. and Rogers, J. (1985), Rapid granulometry of sand using a computer-linked settling-tube, Bulletin 15, Joint UCT/Geological Survey Marine Geoscience Unit.

Clark, P. U., Dyke, A. S., Shakun, J. D., Carlson, A. E., Clark, J., Wohlfarth, B., Mitrovica, J. X., Hostetler, S. W. and McCabe, A. M. (2009), 'The last glacial maximum', *science* **325**(5941), 710–714.

Coleman, F., Diedericks, G., Theron, A. and Lencart e Silva, J. (2021), 'Three-dimensional modelling of the circulation in False Bay, South Africa', *African Journal of Marine Science* **43**(1), 95–118.

Compton, J. S., Mulabisana, J. and McMillan, I. (2002), 'Origin and age of phosphorite from the Last Glacial Maximum to Holocene transgressive succession off the Orange River, South

Africa', *Marine Geology* **186**(3-4), 243–261.

Cooper, J., Green, A. and Compton, J. (2018), 'Sea-level change in southern Africa since the Last Glacial Maximum', *Quaternary Science Reviews* **201**, 303–318.

Daniels, T., Fearon, G., Vilaplana, A., Hewitson, B. and Rautenbach, C. (2022), 'On the importance of wind generated waves in embayments with complex orographic features–A South African case study', *Applied Ocean Research* **128**, 103355.

Darbyshire, M. (1966), The surface waters near the coasts of southern Africa, *in* 'Deep Sea Research and Oceanographic Abstracts', Vol. 13, Elsevier, pp. 57–81.

Davies, J. (1980), *Geographical Variation in Coastal Development*, Geomorphology Texts, 4th edn, Longman.

Day, J. H. (1969), *A Guide to the Marine Life on South African Shores*, Balkema.

De La Cruz, M. (1978), Marine Geophysical and Geological Investigations in Saldanha Bay, Technical Report 9, Joint Geological Survey/University of Cape Town Marine Geoscience Group.

Du Plessis, A. and Glass, J. (1991), 'The geology of False Bay', *Transactions of the Royal Society of South Africa* **47**, 495.

Flemming, B. (1976), 'Rocky Bank - Evidence for a relict wave-cut platform', *Annals of the South African Museum* **71**, 33–48.

Flemming, B. (1982), The Geology of False Bay (Western Cape, South Africa) with special emphasis on modern sediments, Technical Report C/SEA 8253, Csir.

Flemming, B. and Thum, A. (1978), 'The settling tube–a hydraulic method for grain size analysis of sands', *Kieler Meeresforschungen Sonderheft* **4**, 82–95.

Flemming, B. W. (2019), Ripples and dunes: do flumes tell the whole story?, *in* 'MARID VI. Sixth International Conference on Marine and River Dune Dynamics', pp. 89–94.

Folk, R. L. and Ward, W. C. (1957), 'Brazos River bar [Texas]; a study in the significance of grain size parameters', *Journal of Sedimentary Research* **27**(1), 3–26.

Foster, M. S. (2001), 'Rhodoliths: between rocks and soft places', *Journal of phycology* **37**(5), 659–667.

Fourie, J.-P., Ansorge, I., Backeberg, B., Cawthra, H. C., MacHutchon, M. R. and van Zyl, F. W. (2015), 'The influence of wave action on coastal erosion along monwabisi beach, cape town', *South African Journal of Geomatics* **4**(2), 96–109.

Gentle, R. (1971), 'Pre-Quaternary geology of the continental shelf between Cape Infanta and Cape Town', *Technical Report, South African National Commission of Oceanographic*

Research, Marine Geology Programme **3**, 13–27.

Gerlach, R. W., Dobb, D. E., Raab, G. A. and Nocerino, J. M. (2002), 'Gy sampling theory in environmental studies. 1. assessing soil splitting protocols', *Journal of Chemometrics: A Journal of the Chemometrics Society* **16**(7), 321–328.

Glass, G. and Gasson, B. (1980), *Geology, morphology, sediment cover and movement*, False Bay Conservation Society Cape Town, South Africa, pp. 15–25.

Glass, J. (1977), 'Deep weathering of the southwestern Cape Granite and Malmesbury Group: palaeoclimatic implications', *Techn. Rep. Joint Geol. Survey/Univ. Cape Town Marine Geosci. Group* **9**, 118–135.

Glass, J. and Du Plessis, A. (1976), The bathymetry of False Bay as an indicator of sea floor geology, *in* 'Proc. 1st interdisciplinary Conf. mar. freshwater Res. S. Afr'.

Grundlingh, M. and Largier, J. (1991), 'Physical oceanography of False Bay: a review', *Royal Society of South Africa. Transactions TRSAAC,* **47**(4/5).

Grundlingh, M. and Potgieter, E. (1993), 'Unique thermal record in False Bay', *South African Journal of Science* **89**, 510–512.

Haughton, S. H. (1933), *The Geology of Cape Town and Adjoining Country...*, Geological Survey.

Hay, E. R. (1981), A stratigraphic and sedimentological analysis of borehole data from a portion of the cape flats. Honours Thesis.

Hersbach, H., Bell, B., Berrisford, P., Hirahara, S., Horányi, A., Muñoz-Sabater, J., Nicolas, J., Peubey, C., Radu, R., Schepers, D. et al. (2020), 'The era5 global reanalysis', *Quarterly Journal of the Royal Meteorological Society* **146**(730), 1999–2049.

Ingram, R. L. (1965), 'Facies maps based on the megascopic examination of modern sediments', *Journal of Sedimentary Research* **35**(3), 619–625.

Johansen, H. W. (2018), *Coralline algae: a first synthesis*, CRC press.

Jury, M. R. (2020), 'Coastal gradients in False Bay, south of Cape Town: what insights can be gained from mesoscale reanalysis?', *Ocean Science* **16**(6), 1545–1557.

Kidd, R. B., Simm, R. W. and Searle, R. C. (1985), 'Sonar acoustic facies and sediment distribution on an area of the deep ocean floor', *Marine and Petroleum Geology* **2**(3), 210–221.

Kilburn, R. and Rippey, E. (1982), *Sea shells of southern Africa*, Macmillan South Africa.

Komar, P. D. and Miller, M. C. (1973), 'The threshold of sediment movement under oscillatory water waves', *Journal of Sedimentary Petrology* **43**(4), 1101 – 1110.

Komar, P. D. and Miller, M. C. (1975), 'On the comparison between the threshold of sediment motion under waves and unidirectional currents with a discussion of the practical evaluation of the threshold: Reply', *Journal of Sedimentary Research* **45**(1).

Li, Y., Yu, Q., Gao, S. and Flemming, B. W. (2020), 'Settling velocity and drag coefficient of platy shell fragments', *Sedimentology* **67**(4), 2095–2110.

Linton, D. L. (1955), 'The problem of tors', *The Geographical Journal* **121**(4), 470–487.

MacHutchon, M. (2015), 'Geophysical monitoring of coastal erosion and cliff retreat of Monwabisi Beach, False Bay, South Africa', *South African Journal of Geomatics* **4**(2), 80–95.

MacHutchon, M., de Beer, C., Van Zyl, F. and Cawthra, H. (2020), 'What the marine geology of Table Bay, South Africa can inform about the western Saldania Belt, geological evolution and sedimentary dynamics of the region', *Journal of African Earth Sciences* **162**, 103699.

Martins, L. and Barboza, E. (2005), 'Sand–gravel marine deposits and grain-size properties', *Gravel* **3**, 59–70.

McManus, D. (1975), 'Modern versus relict sediment on the continental shelf', *Geological Society of America Bulletin* **86**(8), 1154–1160.

Morgans, J. F. C. (1956), 'The benthic ecology of False Bay, with notes on the analysis of shallow-water soft substrata'.

Müller, G. and Gastner, M. (1971), 'The'Karbonat-Bombe', a simple device for the determination of carbonate content in sediment, soils, and other materials', *Neues Jahrbuch für Mineralogie-Monatshefte* **10**, 466–469.

Munsell, A. (1975), *Soil Color Charts*, Macbeth Division of Kollmorgen Corporation, Baltimore, MD, USA.

Pfaff, M. C., Logston, R. C., Raemaekers, S. J., Hermes, J. C., Blamey, L. K., Cawthra, H. C., Colenbrander, D. R., Crawford, R. J., Day, E., Du Plessis, N. et al. (2019), 'A synthesis of three decades of socio-ecological change in False Bay, South Africa: setting the scene for multidisciplinary research and management', *Elementa: Science of the Anthropocene* **7**.

Rautenbach, C., Barnes, M. A. and de Vos, M. (2019), 'Tidal characteristics of South Africa', *Deep Sea Research Part I: Oceanographic Research Papers* **150**, 103079.

Reineck, H.-E. and Singh, I. B. (1980), Current and wave ripples, *in* 'Depositional Sedimentary Environments', Springer, pp. 22–55.

Retief, G. d. F. (1970), 'Sediment transport in Gordon's Bay', *Transactions of the Royal Society of South Africa* **39**(2), 163–182.

Rogers, J. (2018), *Geological Adventures in the Fairest Cape: Unlocking the Secrets of its*

Scenery, Council for Geoscience Pretoria.

Russell-Cargill, W. (1983), Project Hydra: General background to the project development., Technical Report Tv-019-82, Institute for Maritime Technology.

Salonen, N. and Rautenbach, C. (2021), 'Toward nearshore, bathymetry induced wave amplification in False Bay, South Africa', *AIP Advances* **11**(7), 075209.

Scheepers, R. and Schoch, A. (2006), *The Cape Granite Suite*, Geological Society of South Africa, chapter 5, pp. 421–432.

Schoonees, J., Scholtz, D., Van Tonder, A., Moller, J. and Lenhoff, L. (1983), Valsbaai: Veldata verslag, Technical Report C/sea 8219, Council for Scientific and Industrial Research.

Schulze, B. (1965), *Climate of South Africa. Part 8, General Survey*, SA Weather Bureau.

Shipley, A. (1964), 'Some aspects of wave refraction in False Bay', *South African Journal of Science* **60**(4), 115–120.

Simpson, E., Du Plessis, A. and Forder, E. (1970), 'Bathymetric and magnetic traverse measurements in False Bay and west of the Cape Peninsula', *Transactions of the Royal Society of South Africa* **39**(2), 113–116.

Steller, D. L., Riosmena-Rodriguez, R., Foster, M. S. and Roberts, C. A. (2003), 'Rhodolith bed diversity in the Gulf of California: the importance of rhodolith structure and consequences of disturbance', *Aquatic Conservation: Marine and Freshwater Ecosystems* **13**(S1), S5–s20.

Steneck, R. S. (1986), 'The ecology of coralline algal crusts: convergent patterns and adaptative strategies', *Annual Review of Ecology and Systematics* **17**(1), 273–303.

Stephenson, A. (2016), 'Harmonic analysis of tides using TideHarmonics', *URL https//CRAN. R-project. org/package= TideHarmonics* .

Swift, D. J., Stanley, D. J. and Curray, J. R. (1971), 'Relict sediments on continental shelves: a reconsideration', *The Journal of Geology* **79**(3), 322–346.

Terhorst, A. (1988), The seafloor environment off Simon's Town in False Bay, revealed by side-scan sonar, bottom sampling, diver observations and underwater photography, Bulletin 22, Joint Geological Survey and University of Cape Town Marine Geoscience Unit.

Theron, A. and Schoonees, J. (2007), 'Sand transport at and shoreline response to a breakwater attached to a large tidal pool at Monwabisi, Cape Town', *Journal of the South African Institution of Civil Engineering* **49**(2), 2–9.

Theron, J. (1984), 'The geology of Cape Town and environs: Explanation sheets for 3318 CD and DC and 3418 AB, AD and BA', p. 77.

Van Veen, J. (1936), Onderzoekingen in de hoofden in verband met de gesteldheid der neder-

landsche kust, Technical report, Rijkswaterstaat.

Van Zyl, F. (2011), Marine geophysical survey report: Table mountain marine protected area phase 2 (false bay–simons town to cape point), Technical report, Council for Geoscience, Bellville, Cape Town.

Vos, M. d., Vichi, M. and Rautenbach, C. (2021), 'Simulating the Coastal Ocean Circulation Near the Cape Peninsula Using a Coupled Numerical Model', *Journal of Marine Science and Engineering* **9**(4), 359.

Wainman, C., Polito, A. and Nelson, G. (1987), 'Winds and subsurface currents in the False Bay region, South Africa', *South African Journal of Marine Science* **5**(1), 337–346.

Woelkerling, W. J., Irvine, L. and Harvey, A. S. (1993), 'Growth-forms in non-geniculate coralline red algae (Coralliinales, Rhodophyta)', *Australian systematic botany* **6**(4), 277–293.

Woodborne, M. and Flemming, B. (2021), 'Sedimentological evidence for seiching in a swell-dominated headland-bay system: Table Bay, Western Cape, South Africa', *Geo-Marine Letters* .

Yokoyama, Y., Lambeck, K., De Deckker, P., Johnston, P. and Fifield, L. K. (2000), 'Timing of the Last Glacial Maximum from observed sea-level minima', *Nature* **406**(6797), 713–716.